Specific Inhibition of the Distribution of Lobeglitazone to the Liver by Atorvastatin in Rats: Evidence for an rOATP1B2-Mediated Interaction in Hepatic Transport

Chang-Soon Yim, Yoo-Seong Jeong, Song-Yi Lee, Wonji Pyeon, Heon-Min Ryu, Jong-Hwa Lee, Kyeong-Ryoon Lee, Han-Joo Maeng, and Suk-Jae Chung

College of Pharmacy and Research Institute of Pharmaceutical Sciences, Seoul National University, 1 Gwanak-ro, Gwanak-gu, Seoul 08826, Republic of Korea (C.-.S. Y., Y.-S. J, S.-Y. L., W. P., H.-M. R., and S.-J. C.)

Korea Institute of Toxicology, 141 Gajeong-ro, Yuseong-gu, Daejeon 305-343, Republic of Korea (J.-H. L.)

Life Science Research Center, Daewoong Pharmaceutical Company Ltd., Yongin-si, Gyeonggi-do, 449-814, Republic of Korea (K.-R. L.)

College of Pharmacy, Gachon University, Yeonsu-gu, Incheon, Republic of Korea (H.-J. M.)

DMD # 74120

Running title: DDIs between LB and ATV in rats

Corresponding Author:

Suk-Jae Chung, Ph. D.

College of Pharmacy and Research Institute of Pharmaceutical Sciences

Seoul National University, 1 Gwanak-ro, Gwanak-gu, Seoul 08826, Republic of Korea.

Tel: +82-2-880-9176, Fax: +82-2-885-8317. E-mail: sukjae@snu.ac.kr

Document Statistics:

Text pages: 36

Tables: 4

Figures: 6

References: 62

Abstract: 239

Introduction: 730

Discussion: 1495

Abbreviations:

ACN: acetonitrile; ANOVA: analysis of variance; ATV: atorvastatin; AUC: the area under the concentration-time curve from time zero to infinity; B/P: blood-to-plasma concentration ratio; BCA: Bicinchoninic acid; BSA: bovine serum albumin; CL: systemic clearance; CYP: cytochrome P450; DDI: drug-drug interaction; DMSO: dimethyl sulfoxide; DPBS: Dulbecco's phosphate buffered saline; f_u: fraction unbound; IC_{50}: half maximal inhibitory concentration; IV: intravenous; J: rate of cellular uptake; KHB: Krebs-Henseleit buffer; K_i: inhibition constant; K_m: Michaelis-Menten constant; K_p: tissue-to-plasma partition coefficient;

2

LB: lobeglitazone; LC: liquid chromatography; MDCK: Madin–Darby canine kidney;

mMATE1: mouse multidrug and toxin extrusion 1; mMRP4: mouse multidrug resistance-

associated protein 4; MRT: mean residence time; MS/MS: tandem mass spectrometry; OATP:

organic anion transporting polypeptide; PBPK: physiologically based pharmacokinetics;

PPAR: peroxisome proliferator-activated receptor; PS: unbound passive diffusional clearance;

SD: Sprague-Dawley; T2DM: type-2 diabetes mellitus; V_{ss}: volume of distribution at steady

state

DMD # 74120

Abstract

CYP enzymes and hOATP1B1 are reported to be involved in the pharmacokinetics of lobeglitazone (LB), a new PPARγ agonist. Atorvastatin (ATV), a substrate for CYP3A and hOATP1B1, is likely to be co-administered with LB in patients with the metabolic syndrome. We report herein on a study of potential interactions between LB and ATV in rats. When LB was IV-administered with ATV, the systemic clearance (CL; 2.67 ± 0.63 mL/min/kg) and volume of distribution at steady-state (V_{ss}; 289 ± 20 mL/kg) for LB remained unchanged, compared to those of LB without ATV (CL, 2.34 ± 0.37 mL/min/kg; V_{ss}, 271 ± 20 mL/kg). While the K_p of LB was not affected by ATV in most major tissues, the liver K_p for LB was decreased by the co-administration of ATV. The liver K_p values at the steady state for three levels of LB were significantly decreased as the result of the co-administration of ATV. LB uptake was inhibited by ATV in rOATP1B2-overexpressing MDCK cells and in isolated rat hepatocytes *in vitro*. After incorporating the kinetic parameters for the *in vitro* studies into a PBPK model, the characteristics of LB distribution to the liver were consistent with the findings of the *in vivo* study. It thus appears that the distribution of LB to the liver is mediated by the hepatic uptake of transporters such as rOATP1B2, and the carrier-mediated transport is involved in the liver specific DDI between LB and ATV *in vivo*.

DMD # 74120

Introduction

LB, an agonist for PPARγ, is approved in Korea for the treatment of T2DM. Previous studies (Sauerberg *et al.*, 2003; Kim *et al.*, 2004; Lee *et al.*, 2005) indicate that LB has a therapeutic advantage over rosiglitazone and pioglitazone (i.e., clinically approved/used PPARγ agonists with similar structural motifs) in terms of potency for the PPARγ receptor. As a result, an improvement in insulin sensitivity is expected even at a lower dosage (e.g., 0.5 mg/day): The lower dosage of LB is likely to reduce the incidence of adverse effects (Kim *et al.*, 2014).

We previously demonstrated that LB was primarily metabolized by major CYP enzymes, namely CYP 1A2, 2Cs, and 3A4 (Lee *et al.*, 2015a; Lee *et al.*, 2015b), and interacts with the human organic anion transporting polypeptide 1B1 (hOATP1B1) with an IC_{50} value of 2.44 μM (Lee *et al.*, 2015b). This suggests that drug-drug interactions (DDIs) are possible for LB in drug metabolism as well as in its distribution to tissues. Clinical pharmacokinetics studies of LB with other prescription drugs such as warfarin or amlodipine were recently conducted in Korea, without significant differences in the systemic pharmacokinetics of LB being reported after co-administration (Jung *et al.*, 2015; Kim *et al.*, 2015). These studies were designed to study potential changes in the systemic pharmacokinetics of LB when these drugs were co-administered, considering the fact that they are known to share some of the same metabolic pathways of LB (i.e., CYP 1A2, 2C9, and 3A4 with warfarin; CYP3A4 with amlodipine) (Kaminsky and Zhang, 1997; Guengerich *et al.*, 2002). The lack of appreciable differences in the pharmacokinetics indicates that DDI mediated by drug metabolism is less likely for LB.

In addition to DDI caused by the complications in drug metabolism, based on the literature, it is quite clear that DDIs are possible as a result of interactions at the level of drug transporters. For example, it was reported that cyclosporine inhibits the transport of

rosuvastatin to the liver, probably mediated by hOATP1B1, thereby increasing the plasma level of rosuvastatin by 7.1-fold (Simonson *et al.*, 2004). Interestingly, however, evidence for interactions caused by drug transporters may be less obvious and would be difficult to detect in some cases. For example, it was reported that the concentrations of metformin in the liver and kidney are elevated after the co-administration of cimetidine or pyrimethamine probably caused by inhibiting mMATE1 expressed in the liver and kidney of mice (Ito *et al.*, 2012; Shingaki *et al.*, 2015) without any apparent indication of DDI in the systemic pharmacokinetics. It has also been noted that, the concentration for ciprofloxacin in the liver was decreased after the co-administration of 24-nor-ursodeoxycholic acid by inducing the expression of mMRP4 in the basolateral side of the mouse liver (Wanek *et al.*, 2016), while the systemic pharmacokinetics remained unchanged. These results indicate that conventional methods for detecting DDI are not adequate for some interactions involving transporters and that the possibility of DDI needs to be examined in the target tissue. For the case of LB, however, the possibility of transporter-mediated DDI is not known.

ATV, one of the most frequently prescribed statins (Hsyu *et al.*, 2001; Laufs *et al.*, 2016), is reported to be metabolized by CYP3A4 (Park *et al.*, 2008), and is transported by hOATP1B1 and hOATP1B3 (Knauer *et al.*, 2010). It is now well established that hyperlipidemia can occur simultaneously with T2DM (Iglay *et al.*, 2016) and, thus, a combined treatment involving statins and hypoglycemic agents, such as LB, may become necessary clinically (Gu *et al.*, 2010). It is noteworthy that ATV and LB share similar pathways for drug metabolism (CYP3A4) and distribution to tissues (hOATP1B1). Unfortunately, however, the possibility of DDI between ATV and LB does not appear to have been examined.

The objective of this study, therefore, was to determine whether or not DDIs between LB and ATV occur in rats. We were particularly interested in the possibility of DDI at the

6

level of metabolism by CYP3A and the carrier-mediated transport via rOATP1B2 (i.e., ortholog of hOATP1B1 and hOATP1B3) (Hagenbuch and Meier, 2004) in the pharmacokinetics of LB in the absence or presence of ATV co-administration. The findings indicate that, while no apparent interaction between LB and ATV in their systemic pharmacokinetics was found, a significant interaction for the hepatic distribution of LB was found, most likely at the level of the hepatic distribution via rOap1b2, after the co-administration of ATV.

DMD # 74120

Materials and Methods

Chemicals and Reagents

LB (98.5% purity) was kindly provided by Chong Kun Dang Pharmaceuticals (Seoul, Korea). ATV (98% purity) was purchased from Tokyo Chemical Industry (Tokyo, Japan). Glipizide (96% purity), bicinchoninic acid (BCA), bovine serum albumin (BSA), Hanks' balanced salts, sodium bicarbonate, HEPES, and dimethyl sulfoxide (DMSO) were obtained from Sigma-Aldrich (St. Louis, MO). [^{3}H]-Inulin (194 mCi/g) and [^{3}H]-estradiol-17β-D-Glucuronide (specific activity 41.4 Ci/mmol) [both from American Radiolabeled Chemicals (St. Louis, MO)] were also used in this study. SDS and polyethylene glycol 400 were purchased from Georgiachem (Norcross, GA) and Duksan Pure Chemicals (Ansan, Korea), respectively. Dulbecco's modified Eagle's medium, the non-essential amino acid solution, Dulbecco's phosphate buffered saline (DPBS), penicillin/streptomycin, and fatal bovine serum were obtained from Welgene (Daegu, Korea). High-performance liquid chromatography grade acetonitrile (ACN) and formic acid were purchased from Fisher Scientific (Pittsburgh, PA) and Fluka (Cambridge, MA), respectively. An ammonium formate solution [5 M; Agilent Technologies (Santa Clara, CA)] was also used. Pooled male rat liver microsomes and the NADPH-regenerating system solution were purchased from Corning Gentest (Woburn, MA). Zoletil 50® (tiletamine-HCl/zolazepam-HCl) was purchased from Virbac Laboratories (Carros, France) and Rompun® (xylazine-HCl) from Bayer Corp. (Shawnee Mission, KS). All other chemicals were of reagent grade or greater and were used without further purification.

Animals

Male Sprague-Dawley (SD) rats (body weight 240-270 g) (Orient Bio Inc., Seongnam, Korea) were used in all *in vivo* / hepatocyte isolation studies. Experimental protocols

involving the animals used in this study were reviewed and approved by Seoul National University Institutional Animal Care and Use Committee, according to the National Institutes of Health Publication Number 85-23 *Principles of Laboratory Animal Care* revised in 1985.

IV bolus administration study for the identification of systemic DDIs in rats

Overnight fasted male SD rats were anesthetized by an intramuscular administration of 50 mg/kg of tiletamine-HCl/zolazepam-HCl (Zoletil 50[®]) and 10 mg/kg of xylazine-HCl (Rompun[®]). After confirming the induction of anesthesia, the femoral artery (for collecting blood samples) and vein (for administering and supplementing body fluids) were catheterized with polyethylene tubing (PE 50; Clay Adams, Parsippany, NJ), filled with heparinized saline (20 U/mL; for arterial cannulae) and normal saline (for a venous cannulae), respectively. Upon recovery from the anesthesia, four types of dosing solutions (i.e., LB 0.5 mg/mL, LB 0.5 mg/mL with ATV 2.5 mg/mL, ATV 2.5 mg/mL, or ATV 2.5 mg/mL with LB 0.5 mg/mL) were prepared immediately prior to the administration and given intravenously to rats by a bolus injection. The vehicle for the dosing solutions consisted of DMSO / polyethylene glycol 400 / saline (0.5:4:5.5, v/v/v) and the injection volume was 2 mL/kg. Blood samples (150 μL for each sample) were collected from the arterial catheter at 0, 5, 15, 30, 60, 120, 240, 360, and 480 min (for the study of LB pharmacokinetics) or at 0, 5, 15, 30, 60, and 120 min (for the study of ATV pharmacokinetics) after the administration. Immediately after the blood collection, an identical volume of saline to the volume of the blood sample was given to the animal to compensate for fluid loss. The plasma fraction was separated from blood samples by centrifugation (16,100 g for 5 min at 4°C) and stored at -80°C until used in a liquid chromatography-tandem mass spectrometry (LC-MS/MS) assay for LB and ATV (see below).

IV bolus administration study for the identification of DDIs in rat tissues

Overnight fasted male SD rats were anesthetized and catheterized as described above. Upon recovery from the anesthesia, four types of dosing solutions (i.e., LB 0.5 mg/mL, LB 0.5 mg/mL with ATV 2.5 mg/mL, ATV 2.5 mg/mL, or ATV 2.5 mg/mL with LB 0.5 mg/mL) were similarly prepared and intravenously administered to rats by a bolus injection. The animals were sacrificed at 30, 60, 120, or 240 min after the administration, and tissue (i.e., lungs, adipose, brain, heart, kidneys, muscle, liver, spleen, and gut) samples were collected. In this study, samples of trunk blood were also collected. After tissue isolation, the samples were washed four times with ice-cold DPBS and weighed. Twice the volume of the tissue weight of DPBS was then added for homogenization [Ultra Turrax homogenizer (IKA, Staufen, Germany)]. The mixture was then stored at -80°C until used in determining the concentration of LB and ATV.

When it was necessary to determine the volume of trapped blood in tissue samples, rats were intravenously injected with a solution of inulin containing a trace amount of [^{3}H]-inulin in normal saline (injection volume: 1 mL/kg). Blood samples were collected at 0.5 min, the animals immediately sacrificed by cervical dislocation and tissue samples collected. Blood samples were then centrifuged at 10,770 g for 10 min and the supernatant collected. For tissue samples, approximately 100 mg of tissue sample was weighed and digested with 2 mL of soluene-350 (Perkin-Elmer Life and Analytical Sciences, Waltham, MA). Hydrogen peroxide (200 μL) (35%, Junsei Chemical, Japan) was then added and the resulting sample incubated overnight at room temperature to prevent quenching (Saito *et al.*, 2001). Aliquots of plasma (50 μL) or tissue sample were mixed with Ultima Gold (Perkin-Elmer), and the radioactivity of the sample was determined by liquid scintillation counting (Tri-Carb 3110TR Liquid Scintillation Analyzer, Perkin-Elmer). Considering the possibility that inulin might not be distributed to erythrocytes (Gaudino and Levitt, 1949)**,** the estimated trapped plasma volume was subsequently divided by 0.55 (i.e., 1-hematocrit). In all subsequent studies where

a tissue concentration of drugs was reported, the concentration found in the sample was corrected by subtracting the portion in the trapped blood volume.

IV Infusion study of LB with and without ATV in rats

When it was necessary to further determine the distribution of LB to the liver, a constant LB concentration in the plasma was achieved by IV infusion and the liver concentration determined in the absence and presence of the co-administration of ATV. Thus, overnight fasted male SD rats, weighing 240-270 g, were anesthetized and catheterized, as described above. After recovering from the anesthesia, LB was intravenously infused to rats at the rate of 50, 250, or 1000 ng/min along with or without ATV solution [10 μg/10 μL/min; DMSO / polyethylene glycol 400 / saline (0.5:2:7.5, v/v/v)] using an infusion pump (Harvard, Holliston, MA). Blood samples (150 μL) were collected from the catheter connected to the artery at 30, 60, 120, 240, 300, and 360 min. Upon collecting the last blood sample, the animals were sacrificed and a liver sample collected. The plasma and liver samples were processed for analysis as described above.

Determination of blood-to-plasma concentration ratio and plasma protein binding of LB

LB was added to fresh blank blood at final concentrations of 0.1, 1, or 10 μM, and the mixture incubated at 37°C in a water bath for 60 min. After the incubation, the mixture was centrifuged (16,100 g) and the plasma was collected as the supernatant: The concentration of LB was then determined by LC-MS/MS analysis to calculate blood-to-plasma concentration ratio.

In this study, the extent of plasma protein binding was also determined for LB by the rapid equilibrium dialysis method, according to the manufacturer's recommended protocol

(Thermo Fisher Scientific, Waltham, MA). Briefly, the plate of the dialysis device was rinsed with 20% ethanol for 10 min. LB [0.1, 0.3, 1, 3, or 10 μM as the final concentration for the rat plasma, 0.5, 5, or 50 μM for rat liver microsomes (see below), 0.5, 1, 2, 5, 10, or 20 μM for 5 μM BSA (see below) in the transport medium (9.7 g/L Hanks' balanced salts, 2.38 g/L HEPES, and 0.35 g/L sodium bicarbonate, pH adjusted to 7.4)] and ATV (final concentration; 0.1, 1, or 10 μM for 5 μM BSA in the transport medium) were added to the medium (i.e., the plasma, the microsomal incubation medium, or the transport medium). Aliquots of the mixture (200 μL) and protein free solution (350 μL) were placed into the sample chamber and the buffer chamber, respectively, and the device was sealed / incubated on a shaker (150 rpm) at 37°C for 4 h. After the completion of the incubation, an aliquot (50 μL) was collected from each side of the chamber. To make sure that the matrix of the samples matched, a 50 μL aliquot of blank medium was then added to the protein free solution sample, and an equal volume of protein free solution was also added to the medium. The resulting sample was then analyzed for LB and ATV to determine the unbound fraction (f_u). In this study, the recovery was found to be between 70% and 100% in all experiments.

Stability of LB in rat liver microsomes

In this study, the metabolic stability of LB with or without ATV in rat liver microsomes was determined. The reaction mixture (total volume of 1 mL) consisted of a NADPH-regenerating solution containing 1.3 mM $NADP^+$, 3.3 mM glucose-6-phosphate, 0.4 U/mL glucose-6-phosphate dehydrogenase, and 3.3 mM $MgCl_2$ as recommended by the manufacturer's protocol. Depending on the study, an aqueous solution [100 mM potassium phosphate buffer (pH 7.4)] containing LB (final concentration in the reaction mixture; 1, 2, 5, 10, 20, or 50 μM) without ATV, or LB (the final concentration; 5 μM) with ATV (the final concentration; 1, 5, 10, 20, 50, 100, or 200 μM) was also added. The concentration of organic

solvent (i.e., DMSO) in the incubation mixture was maintained at under 1% to limit its influence on microsomal enzymes. After pre-incubation (37°C for 10 min), the reaction was initiated by the addition of rat liver microsomes (50 μL; the final microsomal protein concentration at 0.5 mg/mL). Preliminary experiments were carried out to determine the incubation time for the given LB concentrations for a linear rate of LB disappearance (data not shown). Samples were collected (50 μL) at various pre-determined times and the samples were then added with an ice-cold ACN solution (i.e., for the termination of the reaction) containing glipizide (100 ng/mL, internal standard). The concentration of LB in the mixture was determined by LC-MS/MS assay.

rOATP1B2 cloning

The protein coding region of rOATP1B2 (Genbank accession number NM_031650.3) was cloned from a rat total liver mRNA library (Takara Shuzo, Japan). The RNA (1 μg) was reverse transcribed using Primescript 1st strand cDNA Synthesis Kit (Takara) by incubating the mixture at 65°C for 5 min, cooling to 4°C, 42°C for 60 min, heating to 95°C for 5 min and cooling to 4°C. Specific primers for cloning of the rOATP1B2 coding region were 5′-GCTAGCAGTGATTGCAGACGTTCCCA-3′ (sense strand; NheI site underlined) and 5′-AAGCTTGTCCATCCTTGCCCCATTCT-3′ (antisense strand; HindⅢ site underlined). The polymerase chain reaction was performed using Ex taq DNA polymerase (Takara) using the following settings: 30 cycles of denaturation at 94°C for 30 sec, a primer-annealing step at 63°C for 30 sec, and extension at 72°C for 3 min. The amplicon was cloned into pcDNA5/FRT vector (Invitrogen, Carlsbad, CA), and the identity of the insert confirmed by sequencing. The plasmid containing the wild type form of rOATP1B2 was selected and transfected into Madin-Darby Canine Kidney II/FRT (MDCKII/FRT) cells using the FuGENE® transfection reagent. The transfected cells were incubated in the culture medium

containing 0.1 mg/mL hygromycin B (Invitrogen) for several weeks for selection. The expression of rOATP1B2 was confirmed by the reverse transcription polymerase chain reaction in the transfected cells. The functional expression was determined by comparing the uptake of radiolabeled estradiol-17β-glucuronide [a standard substrate of the transporter (Catt ori *et al.*, 2000)] in the transfected cells with that in mock-transfected MDCKII/FRT cells (Supplemental Figure 1). In this study, at least a 60-fold higher uptake was found in rOATP1B2 transfected cells with estradiol-17β-glucuronide. Since the measurements in this study involved uptake across the apical membrane, this observation indicates that the transporter is expressed ubiquitously in the plasma membrane, rather than localized in the basolateral membrane (i.e., endogenous site of expression), in the transfected cells. Protein concentrations were determined by a BCA assay (Smith *et al.*, 1985) and used for the correction of the transport function.

Uptake of LB in rOATP1B2-transfected MDCKII/FRT cells

To determine the kinetic characteristics of rOATP1B2 transport, MDCKII/FRT cells expressing the anion transporter were used. Thus, rOATP1B2 cells were grown in Dulbecco's modified Eagle's medium with 10% (v/v) fatal bovine serum, 1% (v/v) non-essential amino acid solution, 100 units/mL penicillin/streptomycin, and 10 mM HEPES. All cells were kept at 37°C with 5% CO_2 and 95% relative humidity. Cells were seeded in poly-L-ornithine (Sigma-Aldrich) -coated 24-well (2.0 cm^2) cell-culture plates (Corning, NY) in supplemented Dulbecco's modified Eagle's medium at a density of 0.5×10^6 cells/well and then grown in a humidified atmosphere of 5% CO_2 at 37°C for 2 days. Preliminary studies were carried out with LB to determine the appropriate reaction time in rOATP1B2 cells as well as mock cells. In this study, up to 12 min of incubation, the uptake was proportional to the incubation time for LB (Supplemental Figure 2), and, thus, a 10 min incubation time was used in subsequent

studies involving LB and rOATP1B2 expressing cells.

For measurement of LB transport in rOATP1B2 cells, the cells were first washed twice with pre-warmed DPBS and pre-incubated with transport medium containing 2% (final concentration) DMSO (i.e., solubilizing agent for LB). From a pilot experiment, it was found that DMSO up to 2% in the transport medium had no appreciable effect on the function of the transporter (Supplemental Figure 3), consistent with other literature findings (Taub *et al.*, 2002; Da Violante *et al.*, 2002). LB was prepared in DMSO and diluted with 5 μM BSA in transport medium (final DMSO concentration of 2%). The addition of BSA was found to be necessary to suppresses the nonspecific adsorption of the drugs on the experimental apparatus and/or cell surface (Takeuchi *et al.*, 2011). The uptake of LB was measured in six different concentrations ranging from 0.5 to 20 μM (i.e., 0.5, 1, 2, 5, 10, or 20 μM) in rOATP1B2 and in mock cells. After pre-incubation for 10 min at 37°C, the transport medium was removed and replaced with pre-warmed medium containing LB in the presence and the absence of ATV (200 μL). Upon completion of the incubation, the aqueous medium was first aspirated, the cells washed twice with ice-cold DPBS containing 0.1 % BSA (400 μL) and once with ice-cold DPBS (400 μL). The final rinsing solution was then aspirated and 0.1 % (w/v) SDS added to the cell suspension for lysis. A preliminary experiment indicated that the addition BSA up to 3% in the rinsing solution had no effect on the protein concentration in the cell lysate. In addition, the effect of limiting the non-specific binding on the experimental apparatus and/or on cell surface was not statistically different for BSA concentrations ranging from 0.1% to 10% in the rinsing solution (Supplemental Figure 4). The resulting mixture was agitated for 30 min, and an ACN solution containing glipizide (100 ng/mL, internal standard) added. After vortexing for 5 min and centrifugation for 5 min (16,100 g), an aliquot (50 μL) of the supernatant was collected and the concentration of LB in the supernatant determined by LC-MS/MS assay (see below). The transport rate was normalized by the protein

concentration in the sample as determined by a BCA assay. When it was necessary, the number of cells was estimated using the predetermined relationship [y (mg protein/mL) = $0.304 \times 10^6 \cdot x$ (cells/mL) + 0.0335, r^2 = 0.994] between the protein concentration (in mg protein/mL) and the number of cells per mL (in 10^6 cells/mL).

When the inhibitory effect of ATV on the transport function of LB in rOATP1B2 cells was studied, the uptake of LB (5 μM) was determined in the cells in the presence of various concentrations of ATV (i.e., 0, 0.01, 0.1, 1, 10, or 30 μM). The transport medium containing DMSO (2%, final concentration) was prepared and BSA (5 μM, final concentration for minimizing nonspecific binding) was added. After a 10 min incubation at 37°C, the uptake was terminated by aspiration of the transport medium. The cells were then rinsed twice with ice-cold DPBS containing 0.1% BSA (400 μL) and once with ice-cold DPBS (400 μL). Cells were lysed for 30 min in 0.1% (w/v) SDS and the mixture agitated. An ACN solution containing glipizide (100 ng/mL, internal standard) was then added to the mixture. After vortexing for 5 min and centrifugation for 5 min (16,100 g), an aliquot (50 μL) of the supernatant was collected and the concentration of LB determined by an LC-MS/MS assay. The data were normalized by the protein concentration in the sample as determined by BCA assay. Preliminary studies were carried out, in an attempt to determine whether the opening of the tight junction is required for transport in the case of rOATP1B2 expressing cells. Therefore, the cells were pretreated with EDTA according to a literature report [Wang et al (2016)] with minor modifications. Briefly, a Ca^{2+}/Mg^{2+}-free transport medium containing 500 μM EDTA was prepared and rOATP1B2 expressing cells were pretreated for 2 h. The transport experiment was then performed as described above. Although the uptake of LB was slightly increased both in mock and rOATP1B2 expressing cells with the comparable K_m and K_i values, this finding suggests that the kinetic properties of carrier mediated transport are not significantly altered for LB by EDTA pre-treatment. Therefore, we chose to exclude the

EDTA pre-treatment step before the transport experiment to prevent the formation of any possible artifacts resulting from the EDTA pre-treatment.

Uptake of LB in isolated rat hepatocytes

Rat hepatocytes were isolated using the two-step collagenase perfusion method with minor modifications (Kotani *et al.*, 2011). Briefly, under anesthesia, a cannulae was inserted into the portal vein followed by perfusing with a Ca^{2+}/Mg^{2+}-free buffer at the flow rate of 20 mL/min for 5 min. Upon the initiation of the perfusion, the inferior vena cava was dissected to allow the perfusate to exit. When necessary, the perfusion medium was switched to a buffer containing 50 mM $CaCl_2$, and 0.5 mg/mL collagenase (Sigma-Aldrich) at a flow rate of 20 mL/min for 10 min. Hepatocytes from the digested liver were dispersed in fresh perfusion buffer and separated from the connective tissue by filtration through a sterile 50-mesh (the size of the sieve opening of 280 μm). Rat hepatocytes were separated from non-parenchymal cells in the crude hepatocyte fraction as a pellet by centrifugation at 50 g for 5 min. The cells were then resuspended in Krebs-Henseleit buffer (KHB) and centrifuged again at 50 g for 5 min. In this study, hepatocytes having a viability of greater than 80%, as determined by a trypan blue exclusion assay, were used in subsequent experiments. The resulting cell pellet was resuspended in Williams' media E containing 10% (v/v) fetal bovine serum, 1% (v/v) penicillin/streptomycin, and 0.01% (v/v) ITS (i.e., 10 mg/mL insulin, 5.5 mg/mL transferrin, and 5 μg/ml selenium) premix (Sigma-Aldrich) at pH 7.4. The hepatocytes were plated in 24-well collagen I (Sigma-Aldrich)-coated plates at a density of 5 $\times$ 10^5 viable cells per well in 0.5 mL of supplemented Williams' media E. The plate was equilibrated from 5 to 6 h at 37°C in an atmosphere containing 5% CO_2 to allow the cells to adhere to the collagen coated surface.

In this study, hepatocyte uptake was measured for six concentrations of LB (i.e., 0.5,

1, 2, 5, 10, or 20 μM). After approximately 5-6 h of cell plating, the medium was aspirated, and the attached cells were rinsed twice with pre-warmed DPBS. LB was dissolved in KHB containing DMSO (5%, final concentration) and BSA (5 μM, final concentration). In a preliminary study, the addition of DMSO up to a final concentration of 10% did not appear to have an appreciable impact on transport function (Supplemental Figure 5), consistent with previous observations (Da Violante *et al.*, 2002). The transport reaction was initiated by the addition of a KHB solution containing LB (200 μL) on the top of the plate. According to our study (Supplemental Figure 6), the accumulation of LB in the hepatocytes was proportional to the incubation time up to 2 min and this incubation time was used in subsequent studies. Cellular uptake was terminated by aspiration of the transport medium, and, cells rinsed twice with ice-cold DPBS containing 0.1% BSA (400 μL) and followed by an additional washing with ice-cold DPBS (400 μL). The hepatocytes were lysed for 30 min by the addition of 0.1% (w/v) SDS and agitation. An ACN solution containing glipizide (100 ng/mL, internal standard) was then added to the lysate and the concentration of LB determined by a LC-MS/MS assay. When necessary, the transport rate was normalized by the amount of protein in the sample as determined by a BCA assay. The number of hepatocytes was also estimated using the predetermined relationship [y (mg protein/mL) $= 0.600 \times 10^6 \cdot x$ (hepatocytes/mL) $- 0.0072$, $r^2 = 0.998$] between the protein concentration (in mg protein/mL) and the number of hepatocytes per mL (in 10^6 hepatocytes/mL).

For the determination of the inhibitory effect of ATV on the transport of LB in rat isolated hepatocytes, LB (5 μM) uptake was measured in the presence of various concentrations of ATV (i.e., 0, 0.001, 0.01, 0.1, 1, 10, 30, or 100 μM). Thus, the medium was aspirated followed by rinsing twice with pre-warmed DPBS. The DPBS was then aspirated, and the cells pre-incubated for 60 min at 37°C with KHB containing various concentrations of ATV (i.e., 0, 0.001, 0.01, 0.1, 1, 10, 30, or 100 μM) and BSA (5 μM, final concentration).

After pre-incubation for 60 min (Amundsen *et al.*, 2010; Shitara *et al.*, 2013), the medium was switched to KHB containing BSA (5 μM, final concentration) and 5 μM of LB along with various concentrations (i.e., 0, 0.001, 0.01, 0.1, 1, 10, 30, or 100 μM) of ATV. After incubation at 37°C for 2 min, uptake was terminated by aspirating the medium, followed by rinsing twice with ice-cold DPBS containing 0.1% BSA (400 μL) and once with ice-cold DPBS (400 μL). The hepatocytes were lysed for 30 min in 0.1% (w/v) SDS and the mixture agitated. An ACN solution containing glipizide (100 ng/mL, internal standard) was then added to the lysate. The concentration of LB was determined by an LC-MS/MS assay. When necessary, the transport rate was normalized by amount of protein in the sample as determined by a BCA assay.

LC-MS/MS assay for LB and ATV

The concentration of LB and ATV in rat plasma samples, tissue homogenates or cell lysates was determined using an LC-MS/MS assay method as previously described (Lee *et al.*, 2009; Kim *et al.*, 2012) with a minor modification. Briefly, an aliquot (50 μL) of sample was vortex mixed with an ACN solution containing glipizide (100 ng/ml, internal standard) followed by a centrifugation (16,100 g for 5 min at 4°C). An aliquot (5 µL) of the supernatant was directly injected onto the LC-MS/MS. In this study, the LC-MS/MS system was equipped with a Waters e2695 high-performance LC system (Milford, MA) and API 3200 Qtrap mass spectrometer (Applied Biosystems, Foster City, CA). Mobile phase, consisting of (A) 0.1% formic acid in ACN and (B) 10 mM ammonium formate in purified water, was delivered at the flow rate of 0.3 mL/min using a gradient elution involving 30% of A (0 min), from 30% to 80% of A (0–0.5 min), 80% of A (0.5–1.5 min), from 80% to 30% of A (1.5–2 min), and 30% of A (2–5 min). The chromatographic separation was carried out on a reversed phase high-performance LC column (Eclipse XDB-C18, 3.5 µm, 2.1 × 100 mm, Agilent

DMD # 74120

Technologies, Santa Clara, CA) at 25°C while the temperature in the autosampler was maintained at 4°C during the analysis. Samples were ionized using a turbo ion spray interface in the positive ionization mode and monitored at the following Q1/Q3 transitions (m/z): 481.3/258.2 for LB, 559.3/440.4 for ATV and 445.8/320.9 for glipizide. The common source/gas conditions for LB, ATV and glipizide were as follows: The pressure of the curtain gas, ion spray voltage, source temperature, ion source gas 1 and ion source gas 2 were 25 psi, 4500 V, 550°C, 60 psi and 60 psi, respectively. The declustering potentials for LB, ATV, and glipizide were 77.9, 45.0, and 47.5 V, respectively. The entrance potentials were 7.4, 4.0, and 4.0 V, collision energies were 47, 27, and 17 V, and the collision cell exit potentials were 4.0, 6.0, and 8.0 V, respectively. The detector response was linear in the concentration range examined (i.e., 5-5000 ng/mL) for both LB and ATV in the rat plasma samples with inter-/intra-day precisions of less than 10% and an accuracy within 8% of the theoretical value, indicative of a valid assay for LB and ATV. In addition to plasma samples, the calibration curves for LB and ATV in the rat tissue homogenates were linear (i.e., $0.992 \leq r^2 \leq 0.999$ for LB and $0.995 \leq r^2 \leq 0.999$ for ATV, respectively) in the concentration range studied. The concentration of LB in cell lysates were also determined with the linear calibration curves (i.e., $0.998 \leq r^2 \leq 0.999$ in cell lysates from mock and rOATP1B2 cells, and $0.998 \leq r^2 \leq 0.999$ in cell lysates from isolated rat hepatocytes).

Data analysis

In vitro kinetic analysis

When it was necessary, the *in vitro* metabolic kinetic parameters (e.g., K_m, V_{max}, and K_i) were determined by fitting the data to eq. 1 and eq. 2 (Segel, 1975):

$$V = \frac{V_{max} \cdot [S]}{K_m + [S]}$$

(1)

DMD # 74120

$$V = \frac{V_{\max} \cdot [S]}{K_{\mathrm{m}} \cdot (1 + \frac{[I]}{K_{\mathrm{i}}}) + [S]} \tag{2}$$

where V was the rate of metabolic reaction, $V_{\max}$ the maximal rate of metabolism, K_{m} the

Michaelis-Menten constant, K_{i} the inhibition constant, $[S]$ the LB concentration as a substrate,

and $[I]$ the ATV concentration as an inhibitor, respectively.

In addition, the cellular transport rate (J) was estimated from the amount of LB uptake

in cell lysates, divided by the incubation time, and expressed in eq. 3 and eq. 4.

In the case where only passive transport was present,

$$J = PS \cdot [S] \tag{3}$$

In case of parallel passive and carrier-mediated transports,

$$J = \frac{J_{\max} \cdot [S]}{K_{\mathrm{m}} + [S]} + PS \cdot [S] \tag{4}$$

where PS is the unbound clearance via passive diffusion and $[S]$, K_{m}, and $J_{\max}$ are the

unbound concentration of LB, unbound Michaelis-Menten constant, and the maximal rate of

the carrier-mediated transport, respectively. Kinetic parameters (e.g., PS, K_{m}, and $J_{\max}$) were

estimated by the simultaneous fitting of the *in vitro* data to eq. 3 and eq. 4 using nonlinear

regression analysis. The measured value for uptake in mock cells may contain some statistical

variability and the correction may not be adequate in some cases (e.g., resulting in a negative

transport value after the correction). As indicated in the literature (DeLean et al., 1978), a

simultaneous fitting approach may result in more reliable values in estimating *vitro* kinetic

parameters. Therefore, we chose to use this method of kinetic analysis.

When it was necessary to analyze the kinetics of the concentration-dependent

inhibition of LB transport by ATV, eq. 5 was fitted to the in vitro data to estimate the half

maximal inhibitory concentration (IC_{50}). In addition, the K_{i} value was estimated using eq. 6

(Cheng and Prusoff, 1973):

$$R = R_{\max} - (R_{\max} - R_0) \cdot \left(\frac{[I]}{[I] + IC_{50}} \right) \tag{5}$$

$$K_i = \frac{IC_{50}}{\left(1 + \frac{[S]}{K_m}\right)} \tag{6}$$

where R, $R_{\max}$, R_0, $[I]$, $[S]$, and K_m are the ratio of the amount of LB transport to the value for

the control group treated without ATV, the maximum value of R, the minimum value of R, the

ATV concentration, the unbound concentration of LB as a substrate, and unbound Michaelis-

Menten constant, respectively. It has been reported that the adoption of Hill's slope factor in

the Cheng-Prusoff equation may introduce additional errors (Lazareno and Birdsall, 1993).

Therefore, the IC_{50} was estimated without using Hill's slope to minimize additional errors (eq.

5). The Winnonlin® Professional 5.0.1 software (Pharsight Corporation, Mountain View, CA)

was used for the nonlinear regression analysis using the equations described above.

Non-compartmental pharmacokinetic analysis

Standard non-compartmental analyses were carried out using the Winnonlin® to

calculate the pharmacokinetic parameters (Gibaldi and Perrier, 1982) including the area under

the plasma concentration–time curve from time zero to infinity (AUC_{inf}), elimination

clearances (CL), terminal $t_{1/2}$, mean residence time (MRT), and apparent volume of

distribution at steady state (V_{ss}).

The tissue-to-plasma concentration ratio of LB (i.e., K_p) was calculated using the eq. 7

(Sawada *et al.*, 1985) after the administration of an IV bolus of LB and/or ATV to rats.

$$K_p = AUC_{inf,tissue} / AUC_{inf,plasma} \tag{7}$$

where $AUC_{inf,tissue}$ represents the area under the drug concentration–time curve in tissue and

$AUC_{inf,plasma}$ represents the area under the drug concentration–time curve in plasma after the

IV bolus administration. For the calculation of the tissue-to-plasma partition coefficient (K_p),

the contribution of trapped blood in the collected tissue was corrected using the volume of blood trapped in tissue samples.

PBPK modeling and simulation

In this study, a PBPK model (see *Appendix*) was constructed assuming the simultaneous IV bolus administration for LB and ATV. The PBPK model consisted of 9 tissues corresponding to the different tissues of the body (lung, adipose, brain, heart, kidneys, muscle, liver, spleen, and gut) and the tissues were assumed to be connected by the circulatory system (arterial and venous side). Physiological and anatomical variables, required in the PBPK calculation, were obtained from the literature (Brown *et al.*, 1997), [i.e., essentially the default values found Simcyp® software (Jamei *et al.*, 2009), version 15 Release 1 (Simcyp Limited, Sheffield, UK)]. In this calculation, the rate of LB/ATV distribution to tissues, including the liver, was assumed to be perfusion rate-limited and the standard mass balance differential equations were used with minor modifications (Lee *et al.*, 2011) (see *Appendix*).

After confirming the adequacy of the constructed PBPK model (for single IV bolus administration of LB and ATV, respectively) (Supplemental Figure 7) with Simcyp® animal simulator (version 15 Release 1), a simulation was carried out with Berkeley Madonna™ software (version 8.3.18; University of California, Berkeley, CA) since a DDI module for rats was not available in the Simcyp® software. In this study, the fourth order of the Runge-Kutta method was used for the numerical integration.

Statistical analysis

When it was necessary to compare the mean values between/among groups, the unpaired Student's *t* test, or one-way ANOVA, followed by Tukey's *post hoc* test, was used.

In this study, data were expressed as the mean ± S.D. and $p < 0.05$ was accepted as denoting

statistical significance.

Results

DDI between LB and ATV in systemic and tissue pharmacokinetics in rats

The mean plasma concentration-time profiles are shown in Figure 1A for an IV bolus administration to rats at a dose of 1 mg/kg LB with or without the simultaneous administration of ATV at dose of 5 mg/kg: The LB concentration profile in the case of the co-administration of ATV was comparable to that without ATV (Figure 1A). The pharmacokinetic parameters, as estimated from a standard moment analysis, are summarized in Table 1. The systemic clearance (CL) of LB with or without ATV were 2.67 ± 0.63 and 2.34 ± 0.37 mL/min/kg, respectively, and these values were not significantly different from each other. The volume of distribution at steady state (V_{ss}) for LB with and without ATV were 289 ± 20 and 271 ± 20 mL/kg, respectively. Furthermore, the secondary pharmacokinetic parameters for LB, such as AUC_{inf}, $t_{1/2}$, and MRT were not affected by the co-administration of ATV. Similar to the case of LB, the ATV concentrations in rat plasma with or without LB co-administration were not changed, as shown in Figure 1B and the summary of pharmacokinetic parameters for ATV (Table 1). Collectively, these observations suggest that there is no appreciable interaction in their systemic pharmacokinetics when LB and ATV are simultaneously given in rats.

The mean tissue concentration-time profiles for LB (Figure 2A) and ATV (Figure 2B) are depicted in Figure 2 for an IV bolus administration to rats at the LB dose (i.e., 1 mg/kg) with or without the co-administration of ATV (i.e., 5 mg/kg). The tissue-to-plasma partition coefficient (K_p) found in this study, along with the volume of blood trapped in tissues for LB and ATV are listed in Table 2. When LB was administered intravenously without ATV, the liver appeared to be the primary organ for distribution, consistent with our previous findings (Lee *et al.*, 2015b). The estimated $K_{p,liver}$ value for LB was 2.34 in the absence of ATV co-administration, while the value was reduced to 1.55 in the presence of ATV co-administration.

For the case of the distribution of LB to tissues other than the liver, ATV co-administration did not appear to significantly affect the distribution of LB. For the case of ATV without LB co-administration, the liver was found to be one of the primary organs for this distribution (i.e., $K_{p,liver}$ = 97.8 and $K_{p,gut}$ = 125). However, the $K_{p,liver}$ and $K_{p,gut}$ values for ATV were reduced to 65.4 and 64.1, respectively, by the co-administration of LB. These observations suggest that DDIs might be a possibility at the level of drug distribution when LB and ATV are simultaneously administered.

Dose dependency of the liver-to-plasma concentration ratio of LB in rats

In this study, different levels of LB in steady state was attained, and the concentrations of LB in the plasma / the liver determined, in an attempt to examine the dependency of $K_{p,liver}$ on LB dosage and ATV co-administration. The mean plasma concentration–time profiles are shown in Figure 3A for IV infusions of LB to rats at rates of 50, 250, or 1000 ng/min with and without the simultaneous infusion of ATV at a rate of 10 μg/min. For all infusion rates, the concentrations of LB in the plasma for 4, 5, and 6 h of infusion were found to not be statistically different among the three time points for a given rate, confirming that a steady state had been reached by 4 h after the infusion. It was also noted that ATV co-administration did not result in a change in LB concentration in the plasma at a 6 h infusion.

The LB concentration was determined in the liver at 6 h: The liver-to-plasma concentration ratio for LB without ATV co-administration was 3.14 ± 0.46 (at 50 ng/min), 1.55 ± 0.52 (at 250 ng/min), and 0.959 ± 0.259 (at 1000 ng/min) (i.e., $p < 0.001$ by one-way ANOVA), respectively. In addition, the liver-to-plasma concentration ratio for LB with ATV co-administration was 1.38 ± 0.39 (at 50 ng/min), 0.701 ± 0.013 (at 250 ng/min), and 0.714 ± 0.184 (at 1000 ng/min), respectively, indicating that the co-administration of ATV

significantly decreases the liver-to-plasma concentration ratio for LB (Figure 3B). For the case of a 1000 ng/min LB infusion condition, the liver-to-plasma concentration ratio for LB was not further decreased by ATV, probably because the transport of LB would be fully saturated by the high concentration of LB. Collectively, these observations indicate that the distribution of LB to the liver is mediated by saturable transport process(es) and that transport to the liver is inhibited by ATV in rats.

Blood-to-plasma concentration ratio (*B/P*) and plasma protein binding

The *B/P* of LB were 0.631 ± 0.023, 0.611 ± 0.022, and 0.667 ± 0.077 (i.e., no statistical difference, by one-way ANOVA) at concentrations of 0.1, 1, and 10 μM, respectively. Considering the lack of concentration dependency in the distribution to blood cells, the average *B/P* for LB (i.e., 0.636) for the three concentrations was assumed to be representative and the value was used in subsequent calculations.

The fraction of unbound LB in the rat plasma ($f_{u,plasma}$) was also found to be independent in the LB concentration range from 0.3 to 10 μM. The representative (i.e., averaged) $f_{u,plasma}$ value of LB was then calculated as 0.00267 ± 0.00036. The fraction of unbound LB in the microsomal incubation medium ($f_{u,MIC}$) was found to be independent in the concentration range from 0.5 to 50 μM, and the representative $f_{u,MIC}$ value of LB was estimated to be 0.479 ± 0.063. However, the unbound fraction of LB at 5 μM BSA in the transport medium ($f_{u,BSA}$) increased with increasing LB concentration in the range from 0.5 to 20 μM (i.e., approximately 0.111-0.447). For the case of $f_{u,BSA}$ of ATV at 5 μM BSA in the transport medium was found to be independent in the concentration range from 1 to 100 μM, and the representative value for $f_{u,BSA}$ was estimated to be 0.588 ± 0.045. These values were used in subsequent calculations.

DMD # 74120

Stability of LB in the presence and absence of ATV in rat liver microsomes

The concentration-metabolic reaction rate profile for LB in rat liver microsomes is shown in Figure 4A. The Eadie-Hofstee transformation of the data is also presented as an inset in Figure 4A. In general, the metabolic rate decreased proportionally with increasing $V/[LB]$ value, suggesting that a saturable process is involved in the metabolic reaction. As a result, assuming that simple Michaelis-Menten kinetics is involved as shown in eq. 1, a nonlinear regression analysis indicates that the $K_{m,MIC}$ and $V_{max,MIC}$ values are 4.37 ± 0.90 μM and 996 ± 110 nmole/min/mg protein, respectively. The inhibitory effect of ATV on the metabolic reaction rate of LB in rat liver microsomes was also determined (Figure 4B) in this study. Based on a nonlinear regression analysis using eq. 2, the $K_{i,MIC}$ value was estimated to be 27.0 ± 5.7 μM. Using the kinetic characteristics obtained in this study, the estimated extraction ratio was calculated to be 0.03 for LB. Therefore, we assumed that a correction of $K_{p,liver}$ for LB was not necessary and this value is reported without correction.

Uptake of LB in rOATP1B2-transfected MDCK cells and isolated rat hepatocytes

The unbound concentration-uptake rate profile for LB in mock cells and rOATP1B2-cells are shown in Figure 5A. Since both LB and ATV drugs that highly bind to plasma proteins (i.e., $f_{u,plasma}$ values of 0.00267 for LB and 0.0567 for ATV, respectively), it is possible that they might also bind non-specifically to the surfaces of experimental apparatus, thereby causing experimental artifacts. In this study, we chose to include BSA in the incubation medium and washing buffer to prevent / minimize non-specific binding to the experimental apparatus and/or cell surface (Takeuchi *et al.*, 2011). As a result, the $f_{u,BSA}$ values of LB were multiplied by the total LB concentration to estimate the concentration of unbound LB in the transport medium. Using this experimental design and a nonlinear regression analysis, $K_{m,OATP}$ and $J_{max,OATP}$ values were found to be 2.06 ± 0.45 μM and $2.42 \pm$

1.27 pmol/min/10^6 cells, respectively (eqs. 3 and 4).

The profile for the unbound concentration-uptake rate for LB in rat hepatocytes is shown in Figure 5B. Similar to the case of transfected cells, the PS, $K_{m,hepa}$, and $J_{max,hepa}$ values were estimated to be 21.0 ± 6.0 µL/min/10^6 cells, 16.3 ± 10.0 µM, and 637 ± 384 pmol/min/10^6 cells, respectively, (eqs. 3 and 4) based on a nonlinear regression analysis. From the inhibitory effect of ATV on the transport rate of LB in rOATP1B2 cells (Figure 5C) and rat hepatocytes (Figure 5D), a nonlinear regression analysis indicated that the $IC_{50,OATP}$ and $IC_{50,hepa}$ are 0.473 ± 0.278 and 0.984 ± 0.812 µM, respectively. Based on the relationship given by Cheng and Prusoff (Cheng and Prusoff, 1973), the $K_{i,OATP}$ and $K_{i,hepa}$ values were estimated to be 0.296 ± 0.174 and 0.875 ± 0.739 µM by eq. 6.

Simulation of LB pharmacokinetic after single IV dose and DDIs using PBPK model

In this study, we attempted to use a PBPK model to predict the plasma and tissue kinetics of LB at a dose of 1 mg/kg (Figure 2A) using primarily *in vitro* experimental results (Table 3). Our calculations indicate that the profiles for the plasma and liver concentration can be reasonably predicted when LB was given to rats intravenously without the co-administration of ATV. (Figs. 6A and 6B). Accordingly, the ratios of AUC_{plasma} to the AUC_{liver} (i.e., $K_{p,liver}$) were calculated to be 2.18 ± 0.09 (Table 4) from *in vitro* data (i.e., $K_{m,MIC}$, $V_{max,MIC}$, PS, $K_{m,hepa}$, and $J_{max,hepa}$), which is reasonably close to the experimentally determined value (i.e., 2.34, Table 4).

Assuming that the current PBPK model for LB is predictive, the PBPK model for LB may also be used to mimic *in vivo* DDI between LB and ATV by using the metabolic and transport kinetic parameters for LB obtained from *in vitro* studies. The observed and simulated LB concentration profiles for the plasma and liver are presented in Figs. 6A and 6B, and their pharmacokinetic parameters are summarized in Table 4. For the case of the $K_{p,liver}$

value of LB with ATV, the predicted value (1.71) was similar to that based on an

experimental determination (1.55) when the $K_{i,OATP}$ value was used in the calculation.

Discussion

The possibility of DDI occurring between LB and ATV was examined, considering the likelihood of the concurrent development of hyperlipidemia / T2DM (Ervin, 2009) and overlapping metabolic (CYP3A) / transport (rOATP1B2) pathways for the two drugs. No apparent DDI was found (Figure 1 and Table 1) between the two drugs in their respective systemic pharmacokinetics, even though interactions between LB and ATV were detected *in vitro* both at the metabolic level (Figure 4B) and transport (Figs. 5C and 5D). Despite its high lipophilicity, the volume of distribution was limited for LB (i.e., 271 ± 20 mL/kg), likely because it extensively binds to plasma proteins. In addition, the reduction in $K_{p,liver}$ for LB (i.e., from 2.34 to 1.55) by ATV did not appear to be significant in the total V_{ss}, considering the fact that the contribution of the reduced distribution of LB to the liver would be approximately 27 mL/kg, which is relatively small for the V_{ss} of 271 mL/kg. In other clinical DDI studies involving LB with metformin (i.e., T2DM agent), LB with warfarin (i.e., an anticoagulant with narrow therapeutic index), or LB with amlodipine (i.e., an anti-hypertensive agent) (Shin *et al.*, 2012; Jung *et al.*, 2015; Kim *et al.*, 2015), no apparent changes in the systemic pharmacokinetics was found as well. In contrast, however, the liver concentration of LB was significantly decreased by the co-administration of ATV (Figure 2 and Table 2). A concentration-dependent decrease was readily apparent for the $K_{p,liver}$ of LB for different levels of steady state LB concentrations (Figure 3) and the extent of liver distribution was determined. These findings are the first indication of this 'liver-specific' DDI between LB and ATV in rats. Other tissue-specific DDIs have also been noted. A decrease in the concentration of metformin in the liver and kidney was reported, without any apparent change in the systemic pharmacokinetics, for the co-administration of cimetidine or pyrimethamine: This tissue-specific change was mediated by the inhibition of mMATE1 (Ito *et al.*, 2012; Shingaki *et al.*, 2015). In addition, an increase in the concentration of donepezil

in the heart and brain was reported, without any appreciable change in the systemic pharmacokinetics, after the co-administration of cilostazol, probably by the inhibition of the breast cancer resistance protein (Takeuchi *et al.*, 2016).

The metabolic rate of LB was also decreased by ATV (Figure 4), although the $K_{i,MIC}$ for ATV (i.e., 15.0 μM, unbound concentration) as estimated from *in vitro* data was relatively high. Since the estimated unbound liver concentration of ATV *in vivo* would be close to 71.8 nM (calculated from the observed $C_{max,liver}$ of ATV when ATV is administered with LB in the tissue study by multiplying $f_{u,plasma,ATV}/K_{p,liver,ATV}$), the maximum concentration of free ATV in the liver (i.e., 1.27 μM) would still be approximately 12-fold lower than the calculated $K_{i,MIC}$ value, even if all ATV in the plasma is present as the unbound form. Taken together, the hepatic metabolism of LB is not likely to be significantly inhibited by the ATV dose administered in this study. In addition, the reduced metabolic activity by ATV from *in vitro* studies did not appear to be consistent with *in vivo* observations in which a lower hepatic concentration of LB by the co-administration of ATV was found. Therefore, we did not pursue the mechanism responsible for the metabolic interaction between LB and ATV *in vitro* any further.

It is now well established that rOATP1B2 is primarily expressed in the liver in rats and ATV is one of its representative substrates (Knauer *et al.*, 2010). These findings indicate that the transport of LB in rOATP1B2 expressing cells had a $K_{m,OATP}$ of 2.06 ± 0.45 μM with a $K_{i,OATP}$ by ATV of 0.296 ± 0.174 μM (Figure 5A and 5C). The uptake of LB was found to be saturable and inhibited by ATV with $K_{i,hepa}$ values of 0.875 ± 0.739 μM in the study involving isolated rat hepatocytes. Collectively, our observations suggest that the distribution of LB to the liver is mediated by hepatic uptake transporter(s), such as rOATP1B2, and the liver distribution of LB is inhibited by the co-administration of ATV, a rOATP1B2 substrate. As confirmation the rOATP1B2 is involved in liver specific DDI, we found that the $K_{p,liver}$ of

ATV declined from 97.8 to 65.4 by the co-administration of LB (Table 2).

Based on *in vitro* studies, LB appeared to be transported to the liver via passive diffusion and carrier-mediated transport(s). Assuming that a similar process occurs *in vivo*, evaluating the $K_{p,liver,pass}$ of LB, representing the liver-to-plasma concentration ratio for LB by passive diffusion only, was necessary. We used the method of Rogers and Rowland (Rodgers and Rowland, 2006) for this (i.e., 0.794 for LB). Interestingly, the current value was comparable to $K_{p,liver}$ measured from the IV infusion study at the highest dose of LB with ATV (i.e., 0.714 ± 0.184; Figure 3B). The ATV plasma concentration was found to be approximately 4.8 μM and the estimated $K_{i,OATP}$ value by ATV approximately 0.3 μM in rOATP1B2 expressing cells. Therefore, carrier-mediated transport by rOATP1B2 appears to be fully inhibited under the above conditions. In subsequent calculations, the computational estimate was assumed to be adequate and was used.

It has been reported that "albumin-mediated uptake mechanism(s)" in hepatocytes may occur for highly bound drugs such as LB and ATV (Poulin *et al.*, 2016). The calculated $f_{u,plasma,surf}$ value for ATV was found to be approximately 5-fold higher than $f_{u,plasma}$ for ATV (i.e., $f_{u,plasma,surf}$ and $f_{u,plasma}$ for ATV were 0.280 and 0.0567, respectively), indicating that the potency of ATV for inhibiting the hepatic uptake of LB might be underestimated by as much as 5-fold if the $f_{u,plasma}$ of ATV is used instead of $f_{u,plasma,surf}$ of ATV (Poulin and Haddad, 2015). In this study, the simulation using $f_{u,plasma,surf}$, instead of $f_{u,plasma}$, yielded improved predictions (Supplemental Figure 8).

The theoretical $K_{p,liver}$ assuming LB without the co-administration of ATV was calculated to be 2.18 ± 0.09, comparable to the observed $K_{p,liver}$ value (i.e., 2.34). In addition, the estimated $K_{p,liver}$ assuming LB was co-administered with ATV was 1.71 ± 0.13, close to 1.55 under a similar *in vivo* situation. Taken together, the simulated $K_{p,liver}$ values for LB with or without ATV were found to be in reasonable agreement with the observed data. It is

noteworthy that the kinetic calculation was primarily based on parameters obtained from *in vitro* studies using rOATP1B2 expressing cells. Therefore, the liver specific DDI between LB and ATV may due to the interaction of rOATP1B2 between the two drugs. Since rOATP1B2 is known to be functionally analogous to hOATP1B1 (Hagenbuch and Meier, 2003), a similar interaction (e.g., the lack of DDI in systemic exposure while the liver concentration for LB reduced by ATV) may occur between LB and ATV in humans. This aspect of DDI involving LB and ATV warrants further investigation.

While LB was reported to be a PPARγ agonist, it possessed a strong affinity for PPARα (i.e., EC_{50} value of 0.02 μM) (Lee *et al.*, 2007). It was reported that fenofibrate, a PPARα agonist, may improve insulin sensitivity, probably by interactions between the drug and its receptor, as shown in an animal model of diabetes and obesity (Koh *et al.*, 2003). Interestingly, the effective dose of LB was significantly lower than that for rosiglitazone and pioglitazone [i.e., (in effective dose) LB, 0.5 mg/day; rosiglitazone, 2-8 mg/day; pioglitazone, 15-45 mg/day] (Balfour and Plosker, 1999; Hauner, 2002; Park *et al.*, 2014). Therefore, it is possible that the higher potency of LB may be partly mediated by the interaction of LB with PPARα. Assuming this, the liver may be regarded as an additional site of action for LB, since the receptor is highly expressed in the liver (Braissant *et al.*, 2011). Considering that the co-administration of LB and ATV led to a liver-specific decrease in the distribution of the two drugs, efficacy could be affected for the two drugs. In particular, since the liver is likely to be closely linked to the pharmacological activity of the drugs (i.e., the primary site of action for ATV and potentially the secondary site for LB), additional studies may be necessary to confirm the impact of the liver specific DDI on the pharmacological activity.

In conclusion, the co-administration of ATV led to a significant decrease in the liver concentration of LB with no appreciable change in its plasma concentration in rats. Metabolic interactions between LB and ATV appeared to cause only minor kinetic changes and is not

DMD # 74120

likely to account for the liver-specific decrease in LB levels *in vivo*. LB was found to be a substrate for rOATP1B2 and carrier-mediated transport was inhibited by ATV, even at low concentrations. The transport variables obtained from *in vitro* studies and the PBPK model assuming a carrier-mediated transport process in distribution to the liver were adequate for mimicking the *in vivo* pharmacokinetics of LB with or without the co-administration of ATV. Considering that LB and ATV might be used in combination, the liver specific DDI caused by the combination found in this study may be therapeutically relevant.

DMD # 74120

Acknowledgments

DMD # 74120

Authorship Contributions

Participated in research design: Yim and Chung.

Conducted experiments: Yim, Jeong, S.-Y. Lee, Pyeon, and Ryu.

Contributed new reagents or analytic tools: J.-H. Lee.

Performed data analysis: Yim, Jeong, Maeng, and Chung.

Wrote or contributed to the writing of the manuscript: Yim, Jeong, J.-H. Lee, K.-R. Lee,

Maeng, and Chung.

References

Amundsen R, Christensen H, Zabihyan B, and Asberg A (2010) Cyclosporine A, but not
   tacrolimus, shows relevant inhibition of organic anion-transporting protein 1B1-mediated
   transport of atorvastatin. *Drug Metab Dispos* **38**:1499–1504.

Balfour JAB, and Plosker GL (1999) Rosiglitazone. *Drugs* **57**:921–930.

Braissant O, Foufelle F, Scotto C, Dauça M, and Wahli W (2011) Differential expression of
   peroxisome proliferator-activated receptors (PPARs): tissue distribution of PPAR-alpha,
   -beta, and -gamma in the adult rat. *Endocrinology* **137**:354–366.

Brown RP, Delp MD, Lindstedt SL, Rhomberg LR, and Beliles RP (1997) Physiological
   parameter values for physiologically based pharmacokinetic models. *Toxicol Ind Health*
   13:407–484.

Cattori V, Hagenbuch B, Hagenbuch N, Stieger B, Ha R, Winterhalter KE, and Meier PJ
   (2000) Identification of organic anion transporting polypeptide 4 (Oatp4) as a major
   full-length isoform of the liver-specific transporter-1 (rlst-1) in rat liver. *FEBS Letters*
   474:242–245.

Cheng Y-C, and Prusoff WH (1973) Relationship between the inhibition constant (KI) and
   the concentration of inhibitor which causes 50 per cent inhibition (I50) of an enzymatic
   reaction. *Biochemical Pharmacology* **22**:3099–3108.

Da Violante G, Zerrouk N, Richard I, Provot G, Chaumeil JC, and Arnaud P (2002)
   Evaluation of the cytotoxicity effect of dimethyl sulfoxide (DMSO) on Caco2/TC7 colon
   tumor cell cultures. *Biol Pharm Bull* **25**:1600–1603.

DeLean A, Munson PJ, and Rodbard D (1978) Simultaneous analysis of families of

sigmoidal curves: application to bioassay, radioligand assay, and physiological dose-response curves. *Am J Physiol* **235**:E97–102.

Ervin RB (2009) Prevalence of metabolic syndrome among adults 20 years of age and over, by sex, age, race and ethnicity, and body mass index: United States. *National health statistics reports*. **13:**1–8.

Gaudino M, and Levitt MF (1949) INULIN SPACE AS A MEASURE OF EXTRACELLULAR FLUID. *Am J Physiol* **157**:387–393.

Gibaldi M, and Perrier D (1982) *Pharmacokinetics*. New York: M, Dekker.

Gu Q, Dillon CF, and Burt VL (2010) Prescription drug use continues to increase: U.S. prescription drug data for 2007-2008. *NCHS Data Brief* 1–8.

Guengerich FP, Brian WR, Iwasaki M, Sari MA, Baeaernhielm C, and Berntsson P (1991) Oxidation of dihydropyridine calcium channel blockers and analogs by human liver cytochrome P-450 IIIA4. *J Med Chem* **34**:1838-1844.

Hagenbuch B, and Meier PJ (2004) Organic anion transporting polypeptides of the OATP/ SLC21 family: phylogenetic classification as OATP/ SLCO superfamily, new nomenclature and molecular/functional properties. *Pflugers Arch Eur J Physiol* **447**:653–665.

Hagenbuch B, and Meier PJ (2003) The superfamily of organic anion transporting polypeptides. *Biochim Biophys Acta* **1609**:1–18.

Hauner H (2002) The mode of action of thiazolidinediones. *Diabetes/Metab Res Rev* **18**:S10–S15.

Hsyu PH, Schultz-Smith MD, Lillibridge JH, Lewis RH, and Kerr BM (2001)
Pharmacokinetic interactions between nelfinavir and 3-hydroxy-3-methylglutaryl
coenzyme A reductase inhibitors atorvastatin and simvastatin. *Antimicrob Agents
Chemother* **45**:3445–3450.

Iglay K, Hannachi H, Joseph Howie P, Xu J, Li X, Engel SS, Moore LM, and Rajpathak S
(2016) Prevalence and co-prevalence of comorbidities among patients with type 2
diabetes mellitus. *Curr Med Res Opin* **32**:1243–1252.

Ito S, Kusuhara H, Yokochi M, Toyoshima J, Inoue K, Yuasa H, and Sugiyama Y (2012)
Competitive inhibition of the luminal efflux by multidrug and toxin extrusions, but not
basolateral uptake by organic cation transporter 2, is the likely mechanism underlying the
pharmacokinetic drug-drug interactions caused by cimetidine in the kidney. *Journal of
Pharmacology and Experimental Therapeutics* **340**:393–403.

Jamei M, Marciniak S, Feng K, Barnett A, Tucker G, and Rostami-Hodjegan A (2009) The
Simcyp ®Population-based ADME Simulator. *Expert Opin Drug Metab Toxicol* **5**:211–
223.

Jung JA, Lee S-Y, Kim T-E, Kim J-R, Kim C, Huh W, and Ko J-W (2015) Lack of the effect
of lobeglitazone, a peroxisome proliferator-activated receptor-γ agonist, on the
pharmacokinetics and pharmacodynamics of warfarin. *Drug Des Devel Ther* **9**:737–743.

Kaminsky LS, and Zhang ZY (1997) Human P450 metabolism of warfarin. *Pharmacol Ther*
73:67–74.

Kim B, Shin H-S, Kim J-R, Lim K-S, Yoon SH, Yu K-S, Shin S-G, Jang I-J, and Cho J-Y
(2012) Quantitative and Qualitative Analysis of CKD-501, Lobeglitazone, in Human
Plasma and Urine Using LC–MS/MS and Its Application to a Pharmacokinetic Study.

Chromatographia **75**:671–677.

Kim BY, Ahn JB, Lee HW, Kang SK, Lee JH, Shin JS, Ahn SK, Hong CI, and Yoon SS
(2004) Synthesis and biological activity of novel substituted pyridines and purines
containing 2,4-thiazolidinedione. *Eur J Med Chem* **39**:433–447.

Kim CO, Sil Oh E, Kim C, and Park MS (2015) Pharmacokinetic Interaction Between
Amlodipine and Lobeglitazone, a Novel Peroxisome Proliferator-activated Receptor-γ
Agonist, in Healthy Subjects. *Clin Ther* **37**:1999–2006.

Kim SG, Kim DM, Woo J-T, Jang HC, Chung CH, Ko KS, Park JH, Park YS, Kim SJ, and
Choi DS (2014) Efficacy and safety of lobeglitazone monotherapy in patients with type 2
diabetes mellitus over 24-weeks: a multicenter, randomized, double-blind, parallel-group,
placebo controlled trial. *PLoS ONE* **9**:e92843.

Knauer MJ, Urquhart BL, Meyer zu Schwabedissen HE, Schwarz UI, Lemke CJ, Leake BF,
Kim RB, and Tirona RG (2010) Human skeletal muscle drug transporters determine local
exposure and toxicity of statins. *Circ Res* **106**:297–306.

Koh EH, Kim M-S, Park J-Y, Kim HS, Youn J-Y, Park H-S, Youn JH, and Lee K-U (2003)
Peroxisome Proliferator-Activated Receptor (PPAR)-α Activation Prevents Diabetes in
OLETF Rats Comparison With PPAR-γ Activation. *Diabetes* **52**:2331–2337.

Kotani N, Maeda K, Watanabe T, Hiramatsu M, Gong L-K, Bi Y-A, Takezawa T, Kusuhara
H, and Sugiyama Y (2011) Culture period-dependent changes in the uptake of transporter
substrates in sandwich-cultured rat and human hepatocytes. *Drug Metab Dispos*
39:1503–1510.

Laufs U, Karmann B, and Pittrow D (2016) Atorvastatin treatment and LDL cholesterol

41

target attainment in patients at very high cardiovascular risk. *Clin Res Cardiol* **105**:783–790.

Lazareno S, and Birdsall NJ (1993) Estimation of competitive antagonist affinity from functional inhibition curves using the Gaddum, Schild and Cheng-Prusoff equations. *Br J Pharmacol* **109**:1110–1119.

Lee H, Kim B, Ahn J, Kang S, Lee J, Shin J, Ahn S, Lee S, and Yoon S (2005) Molecular design, synthesis, and hypoglycemic and hypolipidemic activities of novel pyrimidine derivatives having thiazolidinedione. *Eur J Med Chem* **40**:862–874.

Lee HW, Ahn JB, Kang SK, Ahn SK, and Ha D-C (2007) Process Development and Scale-Up of PPAR α/γ Dual Agonist Lobeglitazone Sulfate (CKD-501). *Org Process Res Dev* **11**:190–199.

Lee J-H, Ahn S-H, Maeng H-J, Lee W, Kim D-D, and Chung S-J (2015a) The identification of lobeglitazone metabolites in rat liver microsomes and the kinetics of the in vivo formation of the major metabolite M1 in rats. *J Pharm Biomed Anal* **115**:375–382.

Lee J-H, Noh C-K, Yim C-S, Jeong Y-S, Ahn S-H, Lee W, Kim D-D, and Chung S-J (2015b) Kinetics of the Absorption, Distribution, Metabolism, and Excretion of Lobeglitazone, a Novel Activator of Peroxisome Proliferator-Activated Receptor Gamma in Rats. *J Pharm Sci* **104**:3049–3059.

Lee J-H, Woo Y-A, Hwang I-C, Kim C-Y, Kim D-D, Shim C-K, and Chung S-J (2009) Quantification of CKD-501, lobeglitazone, in rat plasma using a liquid-chromatography/tandem mass spectrometry method and its applications to pharmacokinetic studies. *J Pharm Biomed Anal* **50**:872–877.

DMD # 74120

Lee K-R, Chae Y-J, Maeng H-J, Lee J, Kim D-D, Chong S, Shim C-K, and Chung S-J (2011)
Physiologically based pharmacokinetic modeling of SNU-0039, an anti-Alzheimer's
agent, in rats. *J Pharmacokinet Biopharm* **38**:637–651.

Lennernas H (2003) Clinical Pharmacokinetics of Atorvastatin. *Clin Pharmacokinet*
42:1141–1160.

Park J-E, Kim K-B, Bae SK, Moon B-S, Liu K-H, and Shin JG (2008) Contribution of
cytochrome P450 3A4 and 3A5 to the metabolism of atorvastatin. *Xenobiotica* **38**:1240–
1251.

Park MK, Kim T-E, Kim J, Kim C, Yoon SH, Cho J-Y, Jang I-J, Yu K-S, and Lim KS (2014)
Tolerability and pharmacokinetics of lobeglitazone, a novel peroxisome proliferator-
activated receptor-γ agonist, after a single oral administration in healthy female subjects.
Clin Drug Investig **34**:467–474.

Poulin P (2015) A paradigm shift in pharmacokinetic-pharmacodynamic (PKPD) modeling:
rule of thumb for estimating free drug level in tissue compared with plasma to guide drug
design. *J Pharm Sci* **104**:2359–2368.

Poulin P, and Haddad S (2015) Albumin and Uptake of Drugs in Cells: Additional Validation
Exercises of a Recently Published Equation that Quantifies the Albumin-Facilitated
Uptake Mechanism(s) in Physiologically Based Pharmacokinetic and Pharmacodynamic
Modeling Research. *J Pharm Sci* **104**:4448–4458.

Poulin P, Burczynski FJ, and Haddad S (2016) The Role of Extracellular Binding Proteins in
the Cellular Uptake of Drugs: Impact on Quantitative In Vitro-to-In Vivo Extrapolations
of Toxicity and Efficacy in Physiologically Based Pharmacokinetic-Pharmacodynamic
Research. *J Pharm Sci* **105**:497–508.

Poulin P, Kenny JR, Hop CECA, and Haddad S (2012) In vitro-in vivo extrapolation of

clearance: modeling hepatic metabolic clearance of highly bound drugs and comparative

assessment with existing calculation methods. *J Pharm Sci* **101**:838–851.

Rodgers T, and Rowland M (2006) Physiologically based pharmacokinetic modelling 2:

Predicting the tissue distribution of acids, very weak bases, neutrals and zwitterions. *J

Pharm Sci* **95**:1238–1257.

Saito T, Zhang ZJ, Ohtsubo T, Noda I, Shibamori Y, Yamamoto T, and Saito H (2001)

Homozygous disruption of the mdrla P-glycoprotein gene affects blood-nerve barrier

function in mice administered with neurotoxic drugs. *Acta Otolaryngol* **121**:735–742.

Sauerberg P, Bury PS, Mogensen JP, Deussen H-J, Pettersson I, Fleckner J, Nehlin J,

Frederiksen KS, Albrektsen T, Din N, Svensson LA, Ynddal L, Wulff EM, and Jeppesen

L (2003) Large dimeric ligands with favorable pharmacokinetic properties and

peroxisome proliferator-activated receptor agonist activity in vitro and in vivo. *J Med

Chem* **46**:4883–4894.

Sawada Y, Hanano M, Sugiyama Y, and Iga T (1985) Prediction of the disposition of nine

weakly acidic and six weakly basic drugs in humans from pharmacokinetic parameters in

rats. *J Pharmacokinet Biopharm* **13**:477–492.

Segel IH (1975) Enzyme kinetics. **957**, Wiley, New York.

Shin D, Kim T-E, Yoon SH, Cho J-Y, Shin S-G, Jang I-J, and Yu K-S (2012) Assessment of

the pharmacokinetics of co-administered metformin and lobeglitazone, a

thiazolidinedione antihyperglycemic agent, in healthy subjects. *Curr Med Res Opin*

28:1213–1220.

Shingaki T, Hume WE, Takashima T, Katayama Y, Okauchi T, Hayashinaka E, Wada Y, Cui Y, Kusuhara H, Sugiyama Y, and Watanabe Y (2015) Quantitative Evaluation of mMate1 Function Based on Minimally Invasive Measurement of Tissue Concentration Using PET with [(11)C]Metformin in Mouse. *Pharm Res* **32**:2538–2547.

Shitara Y, Takeuchi K, and Horie T (2013) Long-lasting inhibitory effects of saquinavir and ritonavir on OATP1B1-mediated uptake. *J Pharm Sci* **102**:3427–3435.

Simonson SG, Raza A, Martin PD, Mitchell PD, Jarcho JA, Brown CDA, Windass AS, and Schneck DW (2004) Rosuvastatin pharmacokinetics in heart transplant recipients administered an antirejection regimen including cyclosporine. *Clin Pharmacol Ther* **76**:167–177.

Smith PK, Krohn RI, Hermanson GT, Mallia AK, Gartner FH, Provenzano MD, Fujimoto EK, Goeke NM, Olson BJ, and Klenk DC (1985) Measurement of protein using bicinchoninic acid. *Anal Biochem* **150**:76–85.

Takeuchi K, Sugiura T, Umeda S, Matsubara K, Horikawa M, Nakamichi N, Silver DL, Ishiwata N, and Kato Y (2011) Pharmacokinetics and hepatic uptake of eltrombopag, a novel platelet-increasing agent. *Drug Metab Dispos* **39**:1088–1096.

Takeuchi R, Shinozaki K, Nakanishi T, and Tamai I (2016) Local Drug-Drug Interaction of Donepezil with Cilostazol at Breast Cancer Resistance Protein (ABCG2) Increases Drug Accumulation in Heart. *Drug Metab Dispos* **44**:68–74.

Taub ME, Kristensen L, and Frokjaer S (2002) Optimized conditions for MDCK permeability and turbidimetric solubility studies using compounds representative of BCS classes I-IV. *Eur J Pharm Sci* **15**:331–340.

Wanek T, Halilbasic E, Visentin M, Mairinger S, Römermann K, Stieger B, Kuntner C, Müller M, Langer O, and Trauner M (2016) Influence of 24-Nor-Ursodeoxycholic Acid on Hepatic Disposition of [(18)F]Ciprofloxacin, a Positron Emission Tomography Study in Mice. *J Pharm Sci* **105**:106–112.

Wang X, Wang N, Yuan L, Li N, Wang J, and Yang X (2016) Exploring tight junction alteration using double fluorescent probe combination of lanthanide complex with gold nanoclusters. *Sci Rep* **6**:32218.

Watanabe T, Kusuhara H, Maeda K, Kanamaru H, Saito Y, Hu Z, and Sugiyama Y (2010) Investigation of the Rate-Determining Process in the Hepatic Elimination of HMG-CoA Reductase Inhibitors in Rats and Humans. *Drug Metab Dispos* **38**:215–222.

Yun YE, and Edginton AN (2013) Correlation-based prediction of tissue-to-plasma partition coefficients using readily available input parameters. *Xenobiotica*, doi: 10.3109/00498254.2013.770182.

Øie S, and Tozer TN (1979) Effect of Altered Plasma Protein Binding on Apparent Volume of Distribution. *J Pharm Sci* **68**:1203–1205.

Footnotes

DMD # 74120

Legends for Figures

Figure 1. (A) Temporal profiles for the plasma concentration of LB after an IV bolus administration of 1 mg/kg dose of LB alone (●) and 1 mg/kg dose of LB with 5 mg/kg dose of ATV (○) to rats. (B) Temporal profiles for the plasma concentration of ATV after an IV bolus administration of 5 mg/kg dose of ATV alone (●) and 5 mg/kg dose of ATV with 1 mg/kg dose of LB (○) to rats. The data are expressed as the mean ± S.D. of quadruplicate runs in A and pentaplicate runs in B.

Figure 2. (A) Temporal profiles for plasma and tissue concentration of LB after IV bolus administration of 1 mg/kg dose of LB alone (●) and 1 mg/kg dose of LB with 5 mg/kg dose of ATV (○) to rats. (B) Temporal profiles for the plasma and tissue concentration of ATV after IV bolus administration of 5 mg/kg dose of ATV alone (▲) and 5 mg/kg dose of ATV with 1 mg/kg dose of LB (△) to rats. The data are expressed as the mean ± S.D. of triplicate runs.

Figure 3. (A) Temporal profiles for the plasma concentration of LB after an IV infusion at dosing rates of 50 (● for LB alone and ○ for LB with ATV 10 μg/min), 250 (▲ for LB alone and △ for LB with ATV 10 μg/min), and 1000 (◆ for LB alone and ◇ for LB with ATV 10 μg/min) ng/min. (B) Liver-to-plasma concentration ratio of LB at 6 h after an IV infusion at the dosing rates of 50, 250, and 1000 ng/min to rats. Asterisks on black circle indicate statistical differences (**$p < 0.01$ and ***$p < 0.001$) from the lowest LB dose (i.e., by one-way ANOVA, followed by Tukey's *post hoc* test), and asterisks under the white circle indicate statistical differences (*$p < 0.05$ and **$p < 0.01$) from the control (i.e., the absence of ATV) by unpaired Student's *t* test. The data are expressed as the mean ± S.D. of quadruplicate runs.

Figure 4. (A) The concentration-metabolic reaction rate curve for LB in an incubation with rat liver microsomes. The solid line was generated by the best-fit parameters obtained from the nonlinear regression analysis based on Michaelis–Menten kinetics (eq. 2). The inset represents an Eadie–Hosftee plot of the concentration-metabolic reaction rate curve. The solid line indicates the linearly regressed line of the data. (B) The inhibitory effect of ATV on the metabolic reaction rate of LB (5 μM) for an incubation with rat liver microsomes. The solid line was generated by the best-fit parameters obtained from the nonlinear regression analysis based on eq. 3. Each symbol represents the mean ± S.D. of triplicate runs.

Figure 5. (A) The unbound concentration-uptake rate curve for LB in Mock-MDCK cells (●) and rOATP1b2-expressing MDCK cells (○). (B) Unbound concentration-uptake rate curve for LB in rat hepatocytes at 4°C (●) and 37°C (○). The solid lines were generated by the best-fit parameters obtained from the simultaneous nonlinear regression analysis based on eq. 4 and eq. 5, respectively. The inhibitory effect of ATV on the uptake of LB (C) in rOATP1b2-expressing MDCK cells, and (D) rat hepatocytes. The solid line was generated by the best-fit parameters obtained from the nonlinear regression analysis based on eq. 6, respectively. Asterisks indicate statistical difference (**$p < 0.01$ and ***$p < 0.001$) from the control group (i.e., without ATV) by one-way ANOVA, followed by Dunnett's *post hoc* test. Each symbol represents the mean ± S.D. of triplicate runs in A, B, and C, and octuplicate runs in D.

Figure 6. (A) Observed and simulated plasma concentration–time profiles for LB after IV bolus administration of 1 mg/kg dose of LB with or without 5 mg/kg dose of ATV to rats. Black circles, solid line, white circles, and dashed line represent the observed (LB alone), simulated (LB alone), observed (LB with ATV), and simulated (LB with ATV, with the $K_{i,OATP}$ value) plasma concentration of LB, respectively. (B) Observed and simulated liver

concentration–time profiles for LB after IV bolus administration of 1 mg/kg dose of LB with

or without 5 mg/kg dose of ATV to rats. Black circles, solid line, white circles, and dashed

line represent the observed (LB alone), simulated (LB alone), observed (LB with ATV), and

simulated (LB with ATV, with the $K_{i,OATP}$ value) liver concentration of LB, respectively.

Symbols represent the mean ± S.D. of triplicate runs. The input parameters for LB and ATV

are summarized in Table 3.

DMD # 74120

Table 1. Pharmacokinetic parameters for LB and ATV after an IV bolus administration of LB (1 mg/kg dose) with and without the co-administration of 5 mg/kg ATV to rats, and after IV bolus administration of 5 mg/kg dose of ATV with and without 1 mg/kg dose of LB to rats, respectively.

	LB		ATV	
Parameter	LB	LB + ATV	ATV	ATV + LB
AUC_{Inf} (µg · min/mL)	422 ± 55	382 ± 85	57.5 ± 26.6	52.1 ± 16.4
$t_{1/2}$ (min)	99.1 ± 4.7	86.4 ± 10.8	22.3 ± 0.9	22.3 ± 1.8
MRT (min)	117 ± 18	111 ± 19	16.2 ± 1.9	16.3 ± 1.4
CL (mL/min/kg)	2.34 ± 0.37	2.67 ± 0.63	102 ± 41	103 ± 33
V_{ss} (mL/kg)	271 ± 20	289 ± 20	1610 ± 600	1670 ± 537

The data are expressed as the mean ± S.D. of quadruplicate runs for LB and pentaplicate runs for ATV.

DMD # 74120

Table 2. Tissue-to-plasma partition coefficient (K_p) for LB and ATV in rats and the volume of blood trapped in rat tissues.

	LB		ATV		Volume of trapped blood
Tissue	LB	LB + ATV	ATV	ATV + LB	in tissues (mL/g tissue)
Lungs	0.240	0.290	1.34	1.96	0.283 ± 0.035
Adipose	0.216	0.216	0.158	0.335	0.0309 ± 0.0063
Brain	0.0252	0.0296	0.0349	0.0270	0.0176 ± 0.0014
Heart	0.343	0.410	0.400	0.396	0.139 ± 0.004
Kidneys	0.406	0.478	2.51	3.28	0.209 ± 0.083
Muscle	0.109	0.170	0.480	0.586	0.0387 ± 0.0082
Liver	2.34	1.55	97.8	65.4	0.105 ± 0.026
Spleen	0.165	0.170	0.884	0.461	0.0430 ± 0.0209
Gut	0.234	0.196	125	64.1	0.107 ± 0.017

The K_p values are obtained from triplicate runs. The volumes of trapped blood in the tissue are expressed as the mean ± S.D. of triplicate runs.

$K_{p,tissue} = (AUC_{inf,tissue} / AUC_{inf,plasma})$

Table 3. Summary of kinetic parameters for LB and ATV used in PBPK calculation.

Parameter	LB	ATV	Reference/comment
Molecular weight (g/mol)	480.5	558.6	Drug bank. http://www.drugbank.ca
Log P	4.3	5.7	ChemAxon. https://www.chemaxon.com
Compound type	Zwitterions	Monoprotic acid	
pKa (acid)	7.61	4.3	ChemAxon. https://www.chemaxon.com
pKa (base)	3.96		
$f_{u,plasma}$	0.00267	0.0567	Determined[a], Ref. (Watanabe *et al.*, 2010)[b]
B/P	0.636	1.2	Determined[a], Ref. (Watanabe *et al.*, 2010)[b]
Distribution			
K_p	0.0252-2.34	0.0270-97.8	Determined
Distribution to liver			
PS (μL/min/10^6 cells)	21.0 ± 6.0		Determined
$J_{max,hepa}$ (pmol/min/10^6 cells)	637 ± 384		Determined
$K_{m,hepa}$ (μM)	16.3 ± 10.0		Determined
Elimination			
$V_{max,MIC}$ (pmol/min/mg	996		Determined

DMD # 74120

protein)

$K_{m,MIC}$ (μM)	4.37		Determined
$f_{u,MIC}$	0.479	0.557	Determined[a], Ref. (Watanabe *et al.*, 2010)[b]
$CL_{u,int}$ (mL/min)		1530	Calculated using the *CL* value of ATV from IV bolus study with LB co-administration
Inhibition			
$K_{i,MIC}$ (μM)		27.0	Determined
$K_{i,hepa}$ (μM)		0.875 ± 0.739	Determined
$K_{i,OATP}$ (μM)		0.296 ± 0.174	Determined
$f_{u,BSA}$	0.111-0.447	0.588	Determined

[a] for LB

[b] for ATV

Table 4. Observed and simulated pharmacokinetic parameters for LB for an IV bolus administration of 1 mg/kg dose of LB alone and 1 mg/kg dose of LB with 5 mg/kg dose of ATV to rats.

Parameter	Observed		Simulated	
	LB	LB + ATV	LB	LB + ATV
$AUC_{inf,plasma}$ (μg · min/mL)	435	509	493 ± 0.08	492 ± 29[a]
$AUC_{inf,liver}$ (μg · min/mL)	1020	789	1070 ± 46	842 ± 68[a]
$K_{p,liver}$	2.34	1.55	2.18 ± 0.09	1.71 ± 0.13[a]

The simulated data are expressed as the mean ± S.D. of three virtual rats from *in vitro* experiments in triplicate runs.

[a] Values were determined using $K_{i,OATP}$ values. $K_{p,liver}$ values were 1.83 ± 0.22 using $K_{i,hepa}$ values.

Appendix

In this study, the pharmacokinetics of LB was assumed to be adequately explained by taking 9 typical tissues into consideration. Thus, the distribution of LB to the lung compartment may be expressed as:

$$V_{LU} \cdot \frac{dC_{LU}}{dt} = Q_{CO} \cdot \left(C_{VB} - \frac{C_{LU} \cdot B/P}{K_{p,LU}} \right) \tag{A1}$$

where V_{LU} is the volume of lung; C_{LU} is the drug concentration in the lung; Q_{CO} is the cardiac output; C_{VB} is the venous blood concentration of drug; B/P is the blood-to-plasma concentration ratio; and $K_{p,LU}$ is the tissue-to-plasma partition coefficient of the lung.

In the venous blood compartment:

$$V_{VB} \cdot \frac{dC_{VB}}{dt} = Q_{AD} \cdot \frac{C_{LU} \cdot B/P}{K_{p,AD}} + Q_{BR} \cdot \frac{C_{BR} \cdot B/P}{K_{p,BR}} + Q_{HE} \cdot \frac{C_{HE} \cdot B/P}{K_{p,HE}} + Q_{KI}$$

$$\cdot \frac{C_{KI} \cdot B/P}{K_{p,KI}} + Q_{MU} \cdot \frac{C_{MU} \cdot B/P}{K_{p,MU}} + Q_{LI} \cdot \frac{C_{LI} \cdot B/P}{K_{p,LI}} + Q_{SP}$$

$$\cdot \frac{C_{SP} \cdot B/P}{K_{p,SP}} + Q_{GU} \cdot \frac{C_{GU} \cdot B/P}{K_{p,GU}} + Q_{RE} \cdot \frac{C_{RE} \cdot B/P}{K_{p,RE}} - Q_{CO} \cdot C_{VB}$$

$$+ Dose\ rate \tag{A2}$$

where V_{VB} is the volume of the venous blood; Q_{AD}, Q_{BR}, Q_{HE}, Q_{KI}, Q_{MU}, Q_{LI}, Q_{SP}, Q_{GU}, and Q_{RE} are the blood flows to the adipose, brain, heart, kidney, muscle, liver, spleen, gut, and the rest of body, respectively; C_{AD}, C_{BR}, C_{HE}, C_{KI}, C_{MU}, C_{LI}, C_{SP}, C_{GU}, and C_{RE} are the drug concentration of adipose, brain, heart, kidney, muscle, liver, spleen, gut, and the rest of body, respectively; $K_{p,AD}$, $K_{p,BR}$, $K_{p,HE}$, $K_{p,KI}$, $K_{p,MU}$, $K_{p,LI}$, $K_{p,SP}$, $K_{p,GU}$, and $K_{p,RE}$ are the tissue-to-plasma partition coefficient of the adipose, brain, heart, kidney, muscle, liver, spleen, gut, and the rest of the body, respectively. Since the kinetics of the rest of the body were negligible for the pharmacokinetics of both LB and ATV (i.e., V_{ss} calculated by Øie-Tozer equation for the 9 major tissues and plasma accounted for 89.4% and 167% of V_{ss} based on the moment analysis of the plasma concentration profiles of LB and ATV, respectively) (Øie and Tozer,

1979), the $K_{p,RE}$ value was arbitrarily set to be 0.001. *Dose rate* refers the dosing rate of the LB and/or ATV.

In the arterial blood compartment of LB and ATV:

$$V_{AB} \cdot \frac{dC_{AB}}{dt} = Q_{CO} \cdot \left(\frac{C_{LU} \cdot B/P}{K_{p,LU}} - C_{AB} \right) \tag{A3}$$

where V_{AB} is the arterial blood volume; C_{AB} and C_{AP} are the drug concentration in arterial blood and plasma, respectively. In our previous report (Lee et al., 2015), the excretion of LB to the bile was found to be negligible (i.e., 0.31%-0.37% of total dose of LB). Therefore we assumed that the elimination of LB and ATV is mainly by hepatic metabolism (Lennernas, 2003; Lee *et al.*, 2015b).

In the liver compartment of LB and ATV:

$$V_{LI} \cdot \frac{dC_{LI}}{dt} = (Q_{LI} - Q_{SP} - Q_{GU}) \cdot C_{AB} + Q_{SP} \cdot \frac{C_{SP} \cdot B/P}{K_{p,SP}} + Q_{GU} \cdot \frac{C_{GU} \cdot B/P}{K_{p,GU}}$$

$$- Q_{LI} \cdot \frac{C_{LI} \cdot B/P}{K_{p,LI}} - \frac{CL_{u,int} \cdot f_{u,plasma} \cdot C_{LI}}{K_{p,LI}} \tag{A4}$$

Metabolism of LB without ATV:

$$CL_{u,int} = \frac{V_{max,MIC}}{K_{m,MIC} \cdot f_{u,MIC} + \dfrac{f_{u,plasma} \cdot C_{LI}}{K_{p,LI}}} \cdot MPPGL \cdot LW \tag{A5}$$

Metabolism of LB with ATV:

$$CL_{u,int} = \frac{V_{max,MIC}}{K_{m,MIC} \cdot f_{u,MIC} \cdot \left(1 + \dfrac{\dfrac{f_{u,plasma,ATV} \cdot C_{LI,ATV}}{K_{p,LI,ATV}}}{K_{i,MIC} \cdot f_{u,MIC,ATV}}\right) + \dfrac{f_{u,plasma} \cdot C_{LI}}{K_{p,LI}}}$$

$$\cdot MPPGL \cdot LW \tag{A6}$$

Distribution to the liver of LB without ATV:

$$K_{p,LI} = \frac{\left(PS + \dfrac{J_{max,hepa} \cdot HPGL \cdot LW}{K_{m,hepa} + f_{u,plasma,surf} \cdot C_{AP}}\right) \cdot K_{p,LI,pass}}{PS} \tag{A7}$$

Distribution to the liver of LB with ATV:

$$K_{p,LI}$$

$$= \frac{\left(PS + \dfrac{J_{max,hepa} \cdot HPGL \cdot LW}{K_{m,hepa} \cdot \left(1 + \dfrac{f_{u,plasma,surf,ATV} \cdot C_{AP,ATV}}{K_{i,hepa} \cdot f_{u,BSA,ATV}} + f_{u,plasma,surf} \cdot C_{AP}\right)}\right) \cdot K_{p,LI,pass}}{PS} \tag{A8}$$

In the liver compartment of ATV:

$$V_{LI} \cdot \frac{dC_{LI}}{dt} = (Q_{LI} - Q_{SP} - Q_{GU}) \cdot C_{AB} + Q_{SP} \cdot \frac{C_{SP} \cdot B/P}{K_{p,SP}} + Q_{GU} \cdot \frac{C_{GU} \cdot B/P}{K_{p,GU}}$$

$$- Q_{LI} \cdot \frac{C_{LI} \cdot B/P}{K_{p,LI}} \tag{A9}$$

where V_{LI} is the liver volume; $CL_{u,int}$ is the unbound intrinsic clearance; $V_{max,MIC}$ is the maximal rate in the microsomal incubation; $K_{m,MIC}$ is the Michaelis-Menten constant in the microsomal incubation; LW, MPPGL, and HPGL were the liver weight (9 g), microsomal protein per gram liver (46 mg/g liver), and hepatocellularity per gram liver (108 × 10^6 hepatocytes/g liver). For scaling the kinetic parameters from *in vitro* experiments to an *in vivo* situation, the Simcyp® default values were used.

$K_{p,LI,pass}$ is the tissue-to-plasma partition coefficient of the liver with when drug transport into and out of tissue is mediated only by symmetric passive diffusion (i.e., theoretically the ratio of the free fraction in plasma to that in liver; $f_{u,plasma,surf} / f_{u,liver}$), where $f_{u,plasma,surf}$ is the unbound fraction of drug at cell surface in plasma (Poulin *et al.*, 2016), respectively. $K_{p,liver,pass}$ was calculated using mechanistic *in silico* prediction methods (Rodgers and Rowland, 2006) within Simcyp®, and $f_{u,plasma,surf}$ was calculated using the eq. A11 (Poulin *et al.*, 2012; Yun and Edginton, 2013; Poulin *et al.*, 2016):

DMD # 74120

$$f_{\text{u,plasma,surf}} = \frac{PLR \cdot \dfrac{f_{\text{unionized,plasma}}}{f_{\text{unionized,cells}}}}{1 + (PLR - 1) \cdot \dfrac{f_{\text{unionized,plasma}}}{f_{\text{unionized,cells}}}} \tag{A10}$$

where PLR is the plasma to tissue concentration ratio of extracellular binding proteins and the value for the liver was 13.3 (Poulin *et al.*, 2012). The $f_{\text{unionized,plasma}}$ and $f_{\text{unionized,cells}}$ are the fraction of uninonized drugs in plasma and cells. The values of $f_{\text{unionized,plasma}}$ and $f_{\text{unionized,cells}}$ were calculated using the pKa value(s) of each drug, and the physiological pH values on both sides of the membrane (e.g., 7.1 for liver and 7.4 for plasma) based on Hendersone-Hasselbalch equations (Yun and Edginton, 2013; Poulin, 2015).

In other tissue compartments:

$$V_{\text{Tissue}} \cdot \frac{dC_{\text{tissue}}}{dt} = Q_{\text{tissue}} \cdot \left(C_{\text{AB}} - \frac{C_{\text{tissue}} \cdot B/P}{K_{\text{p,tissue}}} \right) \tag{A11}$$

where V_{tissue}, C_{tissue}, and $K_{\text{p,tissue}}$ are the tissue volume, the drug concentration in the tissue, and the tissue-to-plasma partition coefficient, respectively.
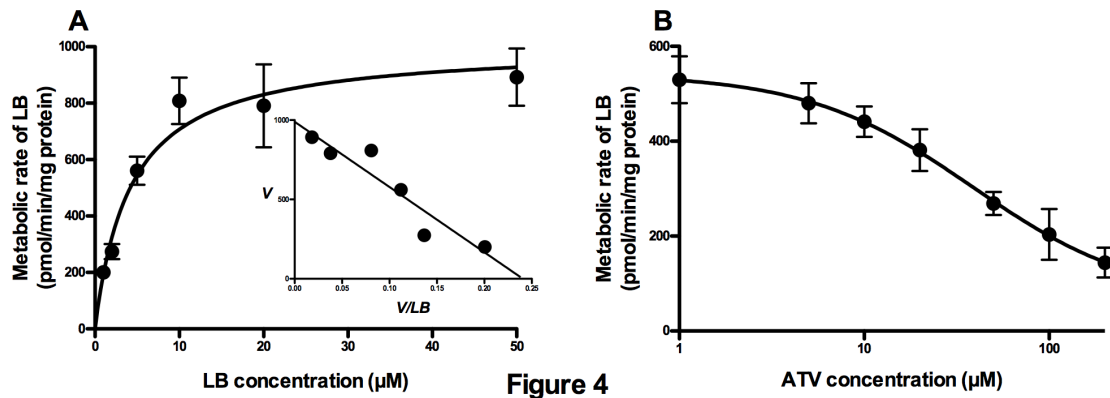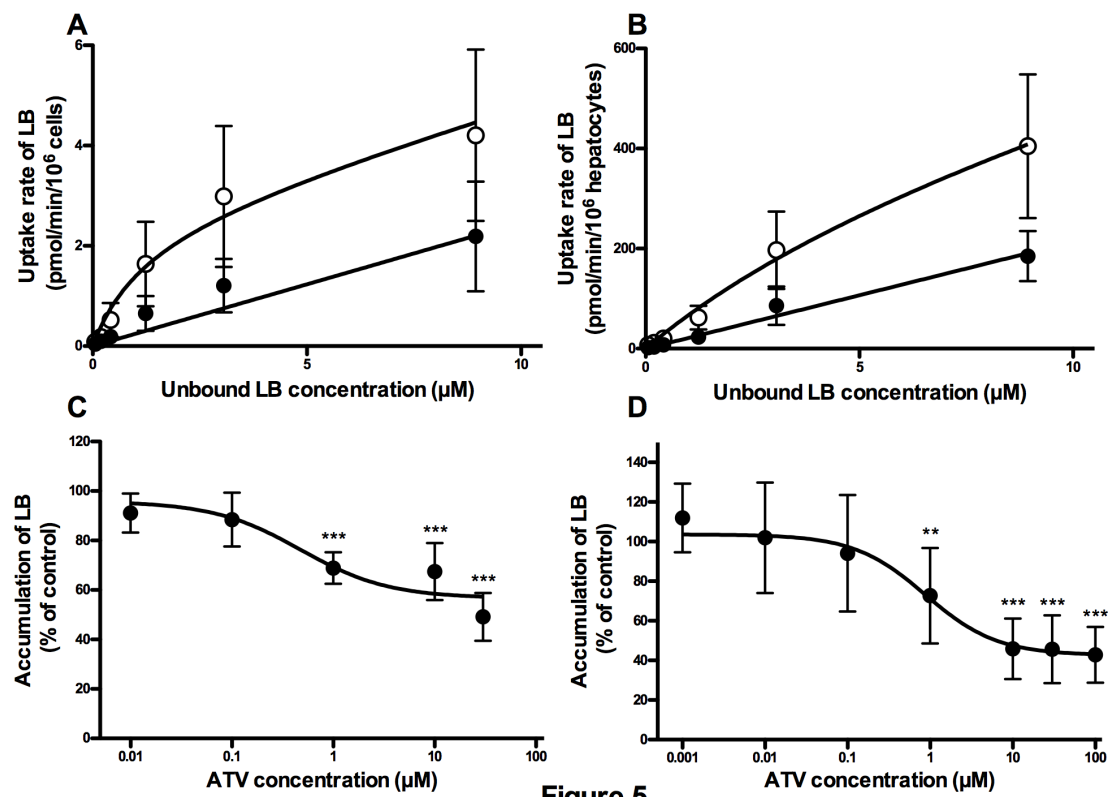
Figure 1
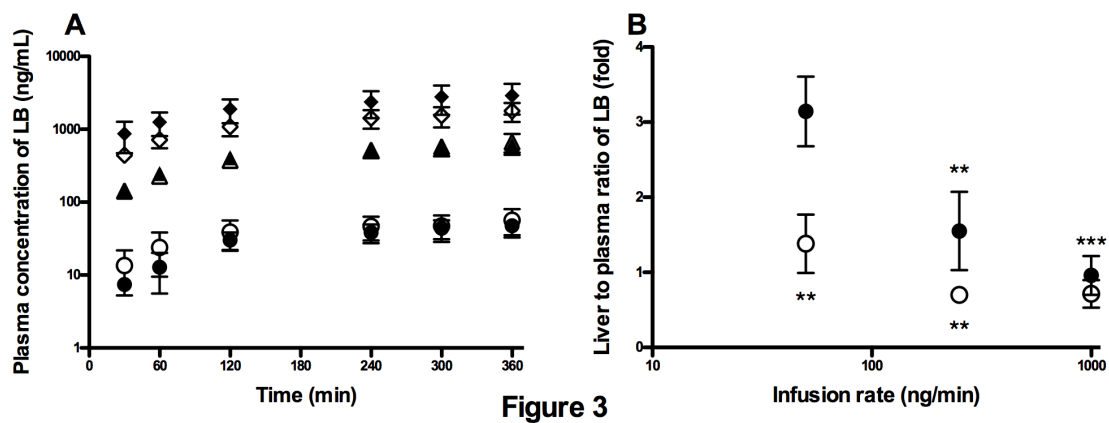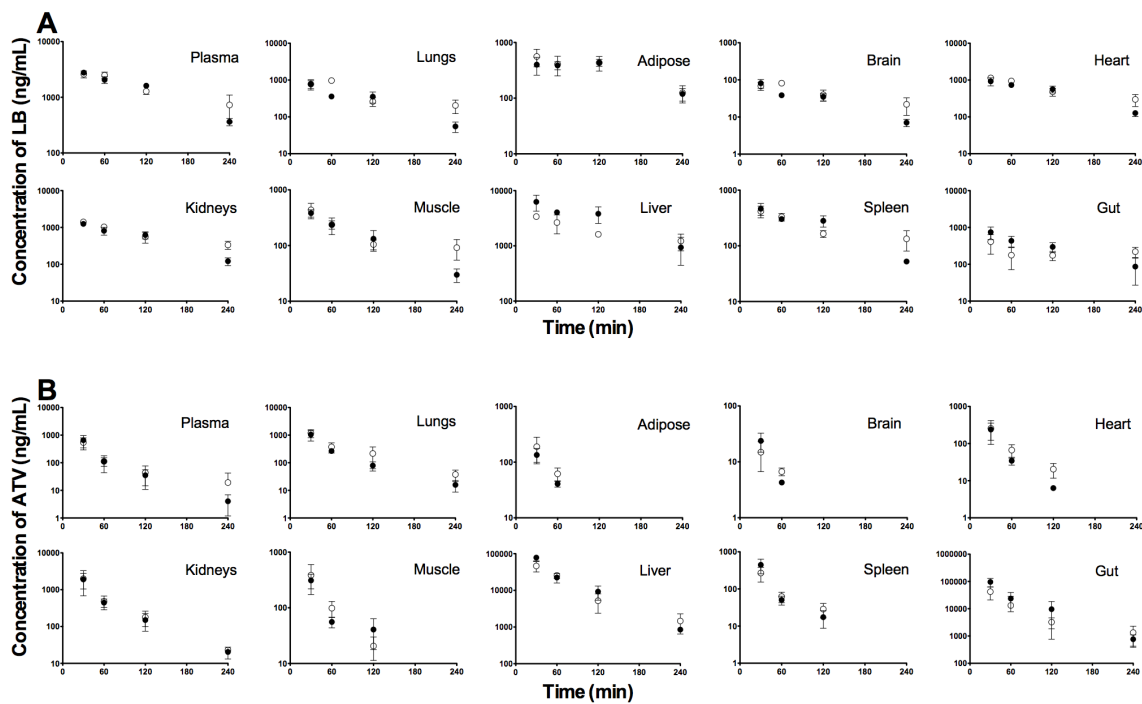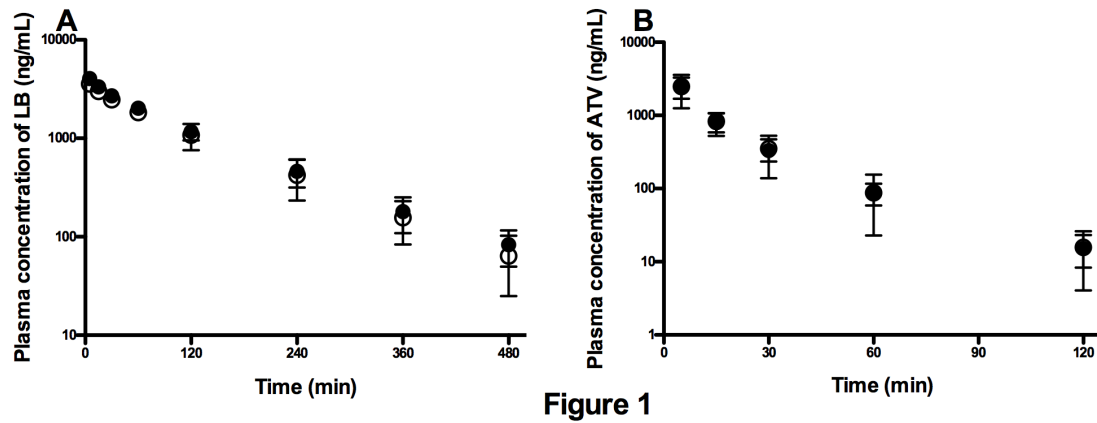
Figure 2

Figure 3

DMD # 74120

Figure 4

Figure 5

DMD # 74120

Figure 6